Thermal Analysis of the ZEPHYR Tape-wound Toroidal Magnet System

M. Söll

IPP 4/195 Dezember 1980

MAX-PLANCK-INSTITUT FÜR PLASMAPHYSIK

8046 GARCHING BEI MÜNCHEN

MAX-PLANCK-INSTITUT FÜR PLASMAPHYSIK

GARCHING BEI MÜNCHEN

Thermal Analysis of the ZEPHYR Tape-wound Toroidal Magnet System

M. Söll

IPP 4/195 Dezember 1980

Die nachstehende Arbeit wurde im Rahmen des Vertrages zwischen dem Max-Planck-Institut für Plasmaphysik und der Europäischen Atomgemeinschaft über die Zusammenarbeit auf dem Gebiete der Plasmaphysik durchgeführt.

Abstract

The thermal analysis of the cryogenically cooled toroidal tape-wound magnet system of ZEPHYR is described.
The methods and calculation techniques developed for this study can generally be used for cryogenic coils which are energized by short current pulses ($\Delta t \sim 10s$). The limitation for the short pulsed coil system is due to the adiabatic heating of the coils, which determines the temperatures in this case where heat conduction plays a minor role.
This report is subdivided into two parts. In the first one analytical calculations are described. Temperatures of (steel-copper) compound conductors are calculated as functions of the initial temperatures before the current pulse is started and of the steel-copper-ratio. The influence of magnetoresistance and nuclear heating are taken into account.
The temperature gradients in the electrical insulation layers are determined by solving the one-dimensional heat conduction equation for a strip with time-dependent boundary conditions.
The second part describes the numerical investigations. The numerical calculations are carried out by using a finite element subdivision of the winding. The temperature profiles within the winding, the ohmic losses, the electric power and the heat deposited are calculated. Finally, optimum cryogenic temperatures T_0 are derived to which the coils should be cooled down between two pulses to minimize the electric power needed by the refrigeration system.

1. Introduction

This report describes the thermal analysis for the tape-wound toroidal field coils of ZEPHYR /1/. The thermal analysis includes: temperature profiles in the coil winding due to ohmic heating and nuclear heating, temperature profiles in the electrical insulators layers, electrical power and total heat depesited in the toroidal coil system.

The toroidal (TF) coil system treated in this report is described in detail in Ref. /1/. The geometry of a TF coil is given in Fig. 1.

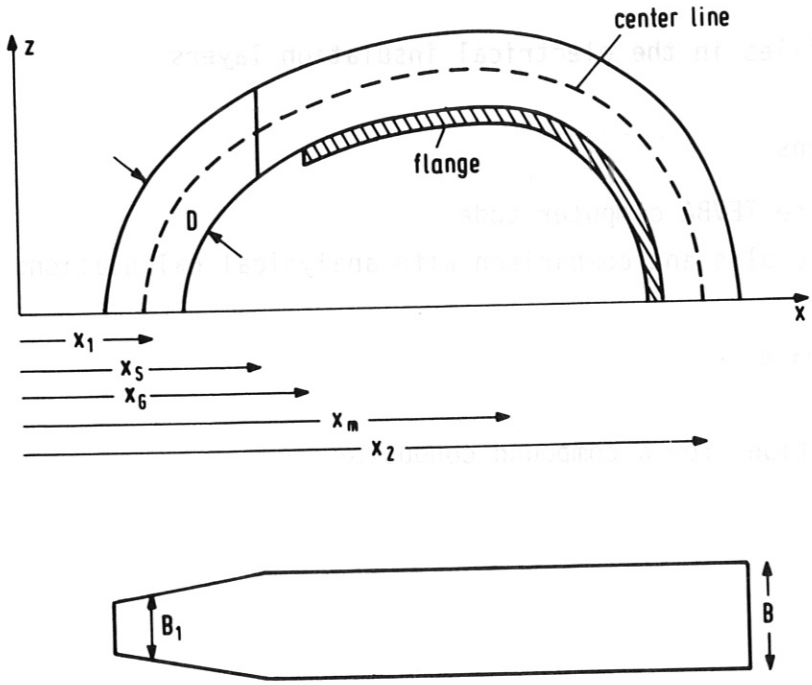

Fig.1 Geometry of the TF-coil for ZEPHYR

x_1 = 0.5725 m
x_2 = 3.17 m
x_s = 1.09 m
x_m = 2.188 m
z_m = 1.25 m
D = 0.345 m
B = 0.432 m
B_1 = 0.212 m
x_G ~1.1 m

The coil is composed of two sections, a C-and a D-shaped section, which join togeter at $x = x_m$, thus forming a bending-free coil configuration /2/.

The TF coil winding is heated by the ohmic losses and by neutrons and gamma radiation.

The time history of the current pulse by which the coil system is energized is shown in Fig. 2. The current rise time is 7 s, the flat-toptime 65 s and the shut-down time 7 s. The total current I_g flowing during the flat-top period in the coils is 61,7 x 10^6 A ($I_g = I_c \cdot n \cdot N$; I_c = current of a conductor,

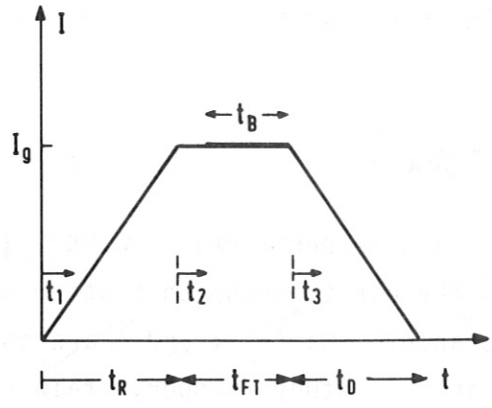

Fig. 2
Current pulse for the TF coil system.
t_R : rise time 7 s
t_{FT} : flat-top time 6.5 s
t_D : shut-clown time 7 s
t_B : burn time 5 s
I_g : total current 61.7×10^6A

n = number of coils, N = number of turns per coil). To ensure mechanical stability, a conductor is composed of a stainless steel (SS) -copper (Cu) tape /1/ with an average SS/Cu ratio $\alpha = 1$.

The average current density $\langle j \rangle$ in the coil throat (plane z = 0; $x_1 - D/2 < x \leq x_1 + D/2$) is $\langle j \rangle = 5.589 \times 10^7$ A/m^2. The high current densities produce high ohmic losses $\rho_e \cdot j^2$ (ρ_e = specific resistivity). In order to sustain the current pulse for 6.5s the coils have to be cooled down to cryogenic temperatures. In this study the temperature range for the initial temperature T_0, the temperature before the current pulse is started, is varied between 30 and 80K. For this temperature interval, supercritical helium and/or liquid nitrogen ($T_0 > 70$K) can be used /1,3,4/ as cooling medium.

In addition to this ohmic heating the winding is also heated by neutron and γ-radiation for pulses with burning plasma. The values for the nuclear energy deposition $q_{n,\gamma}$ are taken from /5/.

2. Analytical calculations

The heat conduction equation for the case that the thermal properties vary with temperature but are independent of position is given by /6/:

$$\rho_m c \frac{\partial T}{\partial t} = \lambda \Delta T + \frac{\partial \lambda}{\partial T} \left\{ \left(\frac{\partial T}{\partial x}\right)^2 + \left(\frac{\partial T}{\partial y}\right)^2 + \left(\frac{\partial T}{\partial z}\right)^2 \right\} + q \quad . \qquad (1)$$

where λ is the thermal conductivity, ρ_m the mass density, c the specific heat, and q the spatial density of heat generation. The heat generation term in our case is composed of two parts, the ohmic heating term $\rho_e j^2$ and

the nuclear energy deposition term $q_{n,\gamma}$. The specific resistivity ρ_e is composed of three parts:

$$\rho_e = \rho_{e0} + \rho_{ep}(T) + \rho_{eB} \quad . \tag{2}$$

where ρ_{e0} is the residual resistivity at low temperatures ($T < 10K$), $\rho_{ep}(T)$ gives the temperature dependence due to the electron-phonon scattering and ρ_{eB} takes into account the magnetoresistance. Data for c and λ are collected in the Appendix for the materials used in this study (copper, stainless steels and electrical insulators).

2.1 Temperature profiles in the conductors

2.1.1 Temperature profiles without magnetoresistance and nuclear heating

The temperatures in a conductor which has to be a composite for mechanical stress reasons /1/ are calculated for adiabatic conditions ($\lambda = 0$). Equation (1) yields for this case

$$\frac{\partial T}{\partial t} = \frac{q}{\rho_m c} \quad . \tag{3}$$

The assumption that the heating process can be calculated under adiabatic conditions is justified by comparing the heat diffusion time t_D for conductor dimensions considered with the effective pulse duration t_{eff}, which yields $t_D > t_{eff}$. The basic equation which has to be solved is given by

$$\frac{\partial T}{\partial t} = \frac{\rho_e(T)}{\rho_m c(T)} \cdot j^2(t) \quad , \tag{4}$$

For deriving analytical solutions a simple formula for the "material function" $f = \rho_e/\rho_m c$ was needed by using the values shown in Figs. A1 and A2. The function f was calculated and is plotted in Fig. 3, which shows the dependence of f on the temperature for a copper conductor ($\alpha=0$) and a composite conductors with $\alpha = 1$ and 2. The f-curve for $\alpha = 0$ is approximated by a linear function f_a ($T > 40K$):

$$f_a = 5/3 \cdot 10^{-9} T \quad . \tag{5}$$

For composite conductors the linear approximation shown in Fig. 3 is given by (see Appendix II)

$$f_a' = \frac{5/3 \cdot 10^{-9}}{1+\alpha} \cdot T \quad . \tag{6}$$

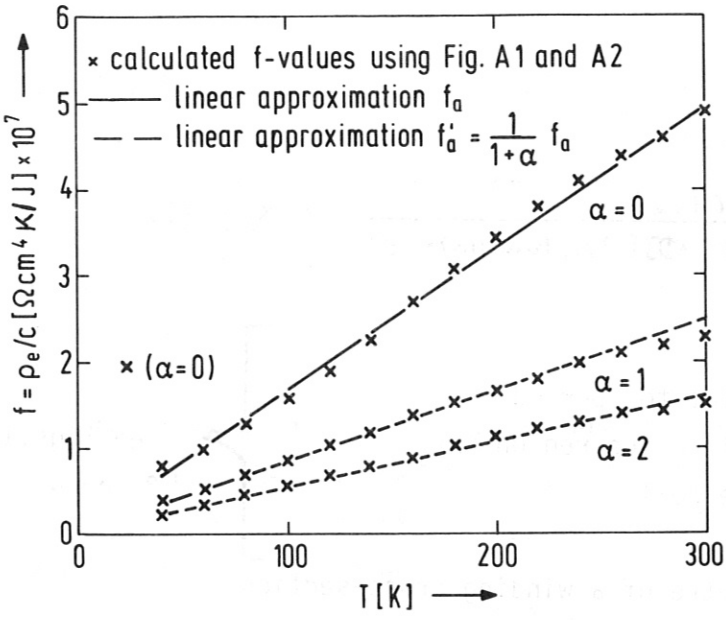

Fig. 3
"Material function" versus temperature for a copper conductor (α = 0, R = 100) and for compound conductors with stainless steel to copper ratio α = 1 and 2. (R = residual resistivity ratio)

Fig. 3 shows that the linear approximation of the "material function" f by relation 6 is accurate enough for rough temperature estimations. The differential equation (4) can now be written in the form.

$$\frac{\partial T}{\partial t} = \frac{5/3 \cdot 10^{-9} \cdot T}{(1+\alpha)} \cdot j^2(t) \,. \qquad (7)$$

This relation (7) is valid for an adiabatic situation with a copper conductor (R = 100; neglecting the magnetoresistance) reinforced by stainless steel; J (t) is the current density in the copper.
The solutions of (7) are

$$T = T_0 e^{\frac{5\cdot 10^{-9}}{3(1+\alpha)} \frac{t_1^3}{3t_R^2} \cdot j_0^2} \qquad 0 \le t \le t_R \,, \qquad (8a)$$

$$T = T_0 e^{\frac{5\cdot 10^{-9}}{3(1+\alpha)} (t_2 + t_R/3) \cdot j_0^2} \qquad t_R < t \le t_R + t_{FT} \,, \qquad (8b)$$

$$T = T_0 e^{\frac{5\cdot 10^{-9}}{3(1+\alpha)} (t_{FT} + t_R/3 + t_D/3) \cdot j_0^2} e^{-\frac{5\cdot 10^{-9}}{3(1+\alpha)} (t_D - t_3)^3 j_0^2 / 3t_D^2} \qquad (8c)$$

$$t_R + t_{FT} < t \le t_R + t_{FT} + t_D \,.$$

Equations (8a) - (8c) describe the dependence of the temperature T on time t during the rise time, the flat-top time and the shut-down time (see Fig. 2). T_0 is the temperature at the beginning of a current cycle and j_0 is the current density in the copper during the flat-top period.
The current density j_0 in the copper is given by

$$j_0 = \frac{I_{sy}(1+\alpha)}{n[B-\Delta B][D-\Delta D]} \qquad x > x_s \,, \qquad (9)$$

$$j_0 = \frac{I_g(1+\alpha)}{n[D-\Delta D][2x_M \tan(\pi/n) - \Delta B]} \qquad x < x_S ; \quad (10)$$

N: total numer of coils
I_g: total current in the flat-top period
B: axial width of the coil in the region $x > x_S$
D: radial thickness of the coil
x_S: tapering edge
x_M: x-coordinate of the centre of a winding cross-section

} see Figs.1 2 and 4

ΔD takes into account the reduction of the conductor area by the high-voltage insulation Δl_H and the electrical insulation between turns, which has the thickness Δl_i. ΔD is given by

$$\Delta D = 2 \cdot \Delta l_H + (N-1) \cdot \Delta l_i \quad , \qquad (11)$$

where N is the number of windings of each coil. ΔB is the reduction of the axial coil width:

$$\Delta B = 2 \cdot \Delta l_H + \Delta l_S \quad , \qquad (12)$$

where Δl_S is the thickness of the spacer plate, placed in the central place of the coil (each coil is composed of two pancakes /1/). If forced cooling in tubes is used, the area reduction by the tubes can be related to an effective Δl_S value. The scheme of the winding cross-section in the coil throat is given in Fig. 4. In the calculation model it is assumed that the current

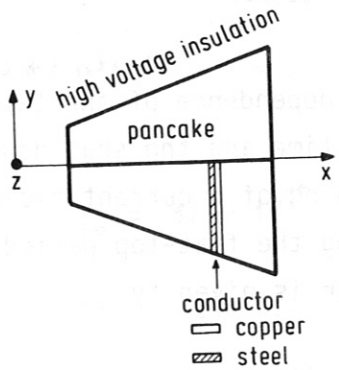

Fig. 4
Scheme of the winding cross-section in the coil throat.

density j is constant over the winding cross-section. For a tape-wound coil with varying winding cross-section in the tapering region this is an ideal assumption because conductors (tapes) then have be made with varying thicknesses in the tapering region. In reality, the coil has to be subdivided into sections where each section has conductors of constant thickness.

In the following figures the temperatures for a conductor in the coil throat where the j-values are highest and for a conductor in the region with parallel coil flanks ($x>x_s$) are shown. The steel-copper ratio α is one. Further values used are:

Δl_H = 0.3 cm,
Δl_i = 0.04 cm,
Δl_s = 0.6 cm,
x_M = 57.25 cm (plane in coil throat)
n = 16 ,
N = 43 ,
B = 43.76 cm,
D = 34.5 cm,
R = 100.

The current density in the coil throat which follows from eq. (10) (x_M = 57.25 cm) is 1.109×10^4 A/cm^2, and for the coil section with $x>x_s$ the current density is 5.624×10^3 A/m^2 [eq. (9)].
The dependence of the temperature T on the time t for a conductor in the coil throat with different initial temperatures T_o (T_o = 40, 60, 80 K) is shown in Fig. 5. The influence of the current density j on the temperature is demonstrated by the curve for a conductor with T_o = 40K placed in the coil section with parallel flanks ($x>x_s$). The reduction of j from 1.109×10^4 A/cm^2 to 5.624×10^3 A/cm^2 leads to a reduction of the temperature increase $\Delta T = T (t = 20.5 s) - T_o$ from 86 K to 14 K.
In the remainder of this section the influence of the steel-to-copper ratio α should be discussed on the basis of eqs. (8a ... 8c). The exponent of the e-function in eqs. (8a - 8c) varies as $(1 + \alpha)$, because j_o^2 scales as $(1 + \alpha)^2$, and the specific heat of the composite conductor as $(1 + \alpha)$. The temperature therefore increase with α as $e^{(1+\alpha)}$. Figure 6 shows the dependence of T on α at the end of the current pulse (t = 20.5 s) for three initial values T_o (40,60 and 80K).

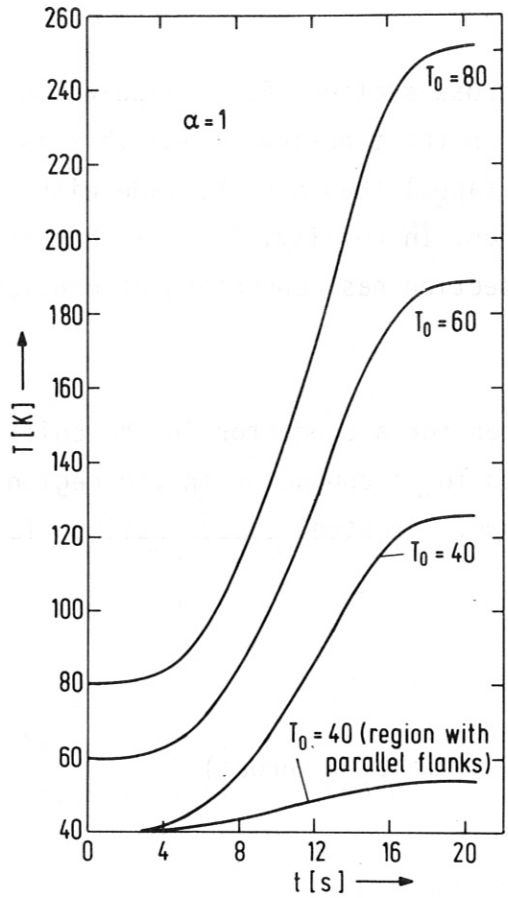

Fig. 5

Temperature variation of a conductor in the coil throat for different initial temperatures T_o and temperature variation for a conductor in the parallel flank region with T_o = 40K (nuclear energy deposition and magnetoresistance not considered)

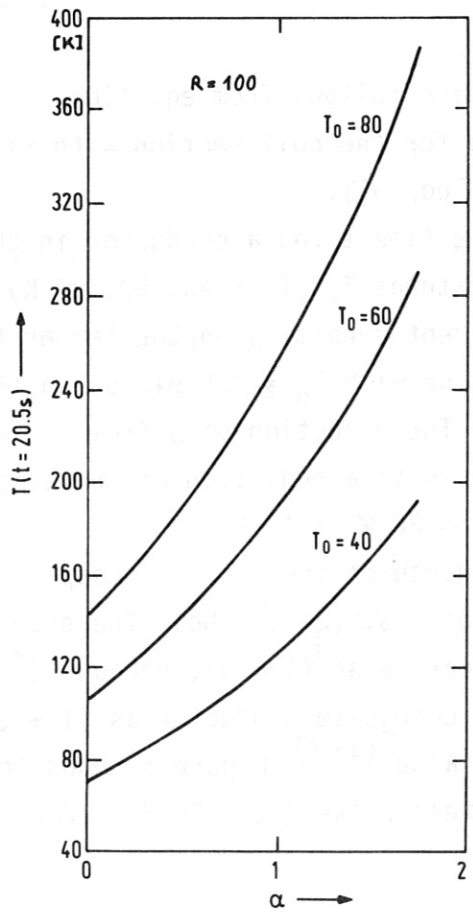

Fig. 6

Dependence of the temperature in the coil throat at the end of the current pulse on the steel-copper ratio α

2.1.2 Temperature profiles with magnetoresistance

As can be seen from Fig. A1, the resistivity ρ_{eB} which results from the magnetoresistance is rather high for windings placed at the inner edge of the coil throat if the temperatures are below 100 K. The magnetic induction at this location is 16.6 T, producing on the copper a ρ_{eB} value of about 0.8×10^{-7} Ω m. This value follows from a linear approxination of the Kohler plot for copper (see Fig. A2) which reads

$$\rho_{eB} = 5 \cdot 10^{-9} \cdot B \quad [\Omega cm], \tag{13}$$

The ρ_e/c function ($\rho_e = \rho_{eo} + \rho_{e\vartheta}(T) + \rho_{eB}$) can be approximated by (see Fig.7)

$$f_a' = \frac{10^{-9}}{(1+\alpha)} (75 + 1.45\,T) \tag{14}$$

for T > 50K.

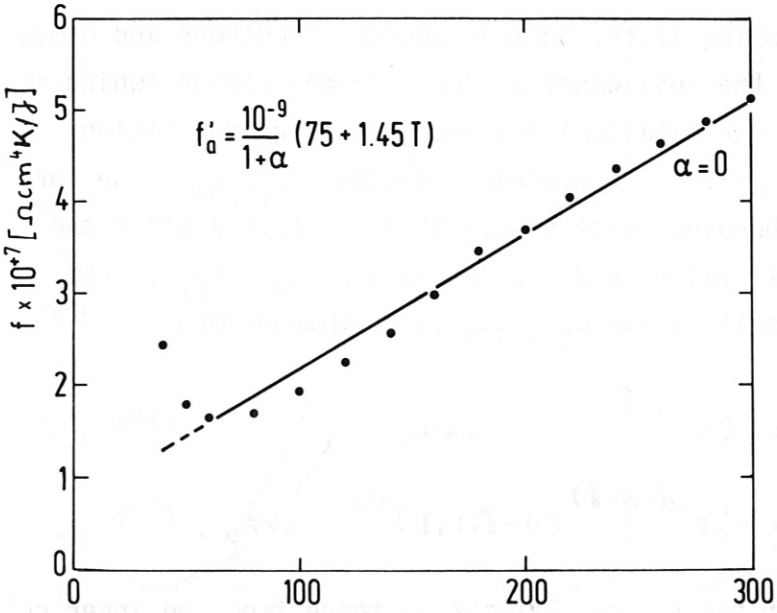

Fig. 7

'Material function"f versus temperature for a copper conductor (α = 0, R = 100) including magneto-resistance

The solution of eq.(4) using eq. (14) as "material function" is

$$T = [T_0 + 51.7]\, e^{\frac{1.45 \cdot 10^{-9}}{(1+\alpha)} \cdot \frac{t_1^3}{3 t_R^2} \cdot j_0^2} - 51.7 \qquad 0 \le t \le t_R \,, \tag{15a}$$

$$T = [T_0 + 51.7]\, e^{\frac{1.45 \cdot 10^{-9}}{(1+\alpha)} (t_2 + t_R/3) \cdot j_0^2} - 51.7 \qquad t_R < t \le t_R + t_{FT} \,, \tag{15b}$$

$$T = [T_0 + 51.7]\, e^{\frac{1.45 \cdot 10^{-9}}{(1+\alpha)} \cdot (t_{FT} + t_R/3 + t_D/3) \cdot j_0^2} \cdot e^{-\frac{1.45 \cdot 10^{-9}}{(1+\alpha)} \cdot \frac{(t_D - t_2)^3}{3 t_D^2} \cdot j_0^2} - 51.7 \tag{15c}$$

$$t_R + t_{FT} < t \le t_R + t_{FT} + t_D \,.$$

(the value 51.7 is the ratio 75/1.45 of the coefficients in the linear f_a-function). The curves in Fig. 8 labelled with A give the temperatures according to the relations (15a)-(15c) for a conductor at the location A shown in the insert of Figure 8. At this point the maximum magnetic induction of 16.6 T occurs. From Fig. 8 the temperatures difference in the coil throut between inner (A) and the outer conductor (C) can be seen. This temperature difference is due to the difference in the magnetic induction B which is assumed to be zero at the outer winding edge. Numerical field calculations show that this assumption is justyfied. The curves C are taken from Fig. 5 (the temperatures are calculated without magnetoresistance). The curves in Fig. 8 show that the temperature difference between the inner and outer conductors in the coil throat increases with decreasing initial temperature.

2.1.3 Temperature profiles with magnetoresistance and nuclear heating

If the plasma is in the burning state, nuclear energy (neutrons and gamma radiation) is deposited in the coil winding. For a former design (which is classified as $C_{1.5/330}$ in our notation) the nuclear energy deposition in the coil was calculated /5/. For the present design ($C_{1.5/345}$) the burn time t_B is 5 seconds. The burning phase starts at 8.5 s (1.5 s after the current has reached its full value) and ends at 13.5 s ($t_R + t_{FT}$). From /5/ the nuclear energy deposition for $C_{1.5/345}$ is estimated to be

$$q_{n,\gamma} = W_0 e^{-\lambda' \delta} \qquad x < x_G \;, \tag{16}$$

$$q_{n,\gamma} = W_0 e^{-\lambda'(d+\delta)} (1 - \delta/1.1D)^{1/2} \qquad x > x_G \;, \tag{17}$$

where d is the thickness of the flange, δ is the distance from the inner coil edge and is the coordinate where the flange begins. The value of W_0 and λ' are 12 W/cm^3 /5/ and 9.61 m^{-1} respectively. The differential equation for the burning plasma phase now reads

$$\frac{\partial T}{\partial t} = f_a' j^2(t) + \frac{q(1+\alpha)}{\rho_m \cdot c(T)} \;, \tag{18}$$

where $\rho_m c$ is the specific heat of the copper in J/cm^{3}K and f_a' is given by eq. (14). To get analytical solution of eq. (18), the specific heat $\rho_m \cdot c(T)$ is approximated by a constant value $\overline{\rho_m c}$ for the temperature interval

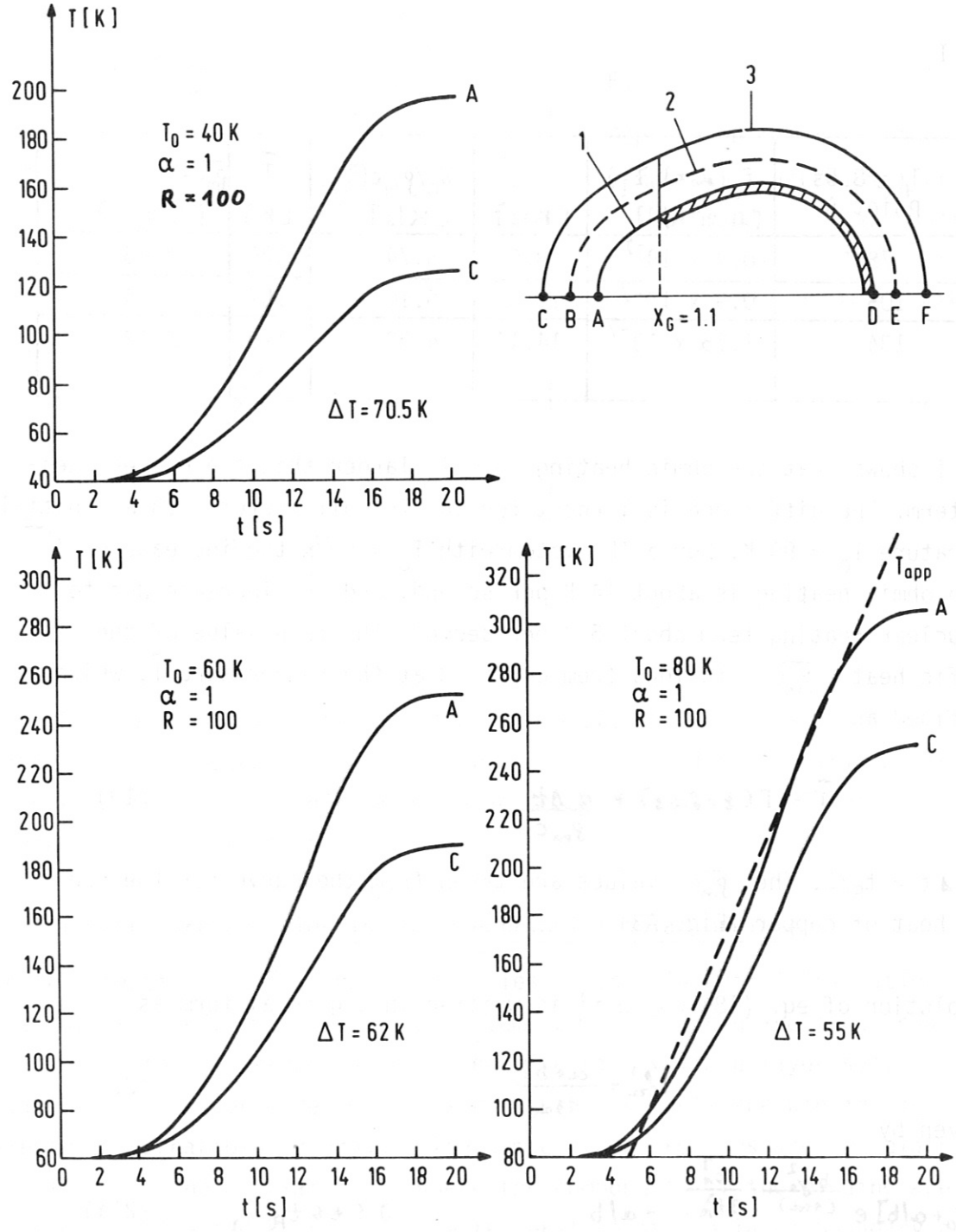

Fig. 8 Temperatures at the inner edge (point A) and at the outer edge (C) of the coil throat. The temperatures in A are calculated taking into account the magnetoresistance.

8.5 s and 13.5 s. To get an idea of the influence exerted by the nuclear heating term $q/\rho_m c\,(T(t = 8.5\ s))$, it is compared with $f_a j^2$ $(t = 8.5\ s)$. This data, which are determined by T values of Fig. 8, are shown in Table I (for position A: $q_{nuc} \equiv W_0$):

Table I

T_o	T_1(t=8.5s) Point A	$f_a(\alpha=1,T_1)$ [$\Omega cm^4 K/J$]	$f_a j^2$ [K/s]	$W_o/\rho_m c(T_1)$ [K/s]	$\bar{T}$ [K]	$\overline{\rho_m c}$= C(T) [$J/cm^3 K$]
40	78	0.7×10^{-7}	8.61	6.74	126	2.65
60	105	0.9×10^{-7}	11.07	5.10	157	2.94
80	134	1.15×10^{-7}	14.14	4.38	190	3.12

Table I shows that the ohmic heating term is larger than the nuclear heating term. The difference is largest for the TF coil system with an initial temperature T_o = 80 K. For a TF system with T_o = 80 K the increase of T due to ohmic heating is about 14 K per second, and the increase due to the nuclear heating term about 5 K per second. The mean value of the specific heat $\overline{\rho_m c}$ follows from curve A3 at the temperature $\bar{T}$, which is defined as

$$\bar{T} = T(t=8.5s) + \frac{q\,\Delta t}{\rho_m c} \qquad (19)$$

with $\Delta t = t_B/2$. The $\overline{\rho_m c}$ -values are taken from the curve for the specific heat of copper (Fig. A3).

The solution of eq. (18) where f_a' is written in a general form as

$$f_a' = \frac{a+bT}{(1+\alpha)} \qquad (20)$$

is given by

$$T = [T_o + a/b]\, e^{\frac{b j_o^2}{(1+\alpha)} \cdot \frac{t_1^3}{3t_R^2}} - a/b \qquad 0 \le t \le t_R\,, \qquad (21a)$$

$$T = [T_o + a/b]\, e^{\frac{b j_o^2}{(1+\alpha)} \cdot (t_R/3 + t_2)} - a/b \qquad t_R < t \le t_R + t_{FT} - t_B\,, \qquad (21b)$$

$$T = \left\{ [T_o + a/b]\, e^{\frac{b j_o^2}{(1+\alpha)} \cdot (t_{FT} - t_B + t_R/3)} + \frac{q(1+\alpha)}{j_o^2 b \overline{\rho_m c}} \right\} e^{\frac{b j_o^2}{(1+\alpha)} t_2'} - a/b - \frac{q(1+\alpha)}{j_o^2 b \overline{\rho_m c}} \qquad 0 < t_2' < t_B\,, \qquad (21c)$$

$$T = \left\{ \frac{q(1+\alpha)}{\overline{\rho_m c} \cdot b j_o^2}\, e^{\frac{b j_o^2}{(1+\alpha)}} \left[e^{\frac{b j_o^2}{(1+\alpha)}} - 1 \right] + [T_o + a/b]\, e^{\frac{b j_o^2}{(1+\alpha)} \cdot (t_{FT} + t_R/3 + t_D/3)} \right\} \cdot e^{-\frac{b j_o^2}{(1+\alpha)} \cdot \frac{(t_D - t_3)^3}{3 t_D^2}} - a/b \qquad t_R + t_{FT} < t \le t_R + t_{FT} + t_D\,.$$

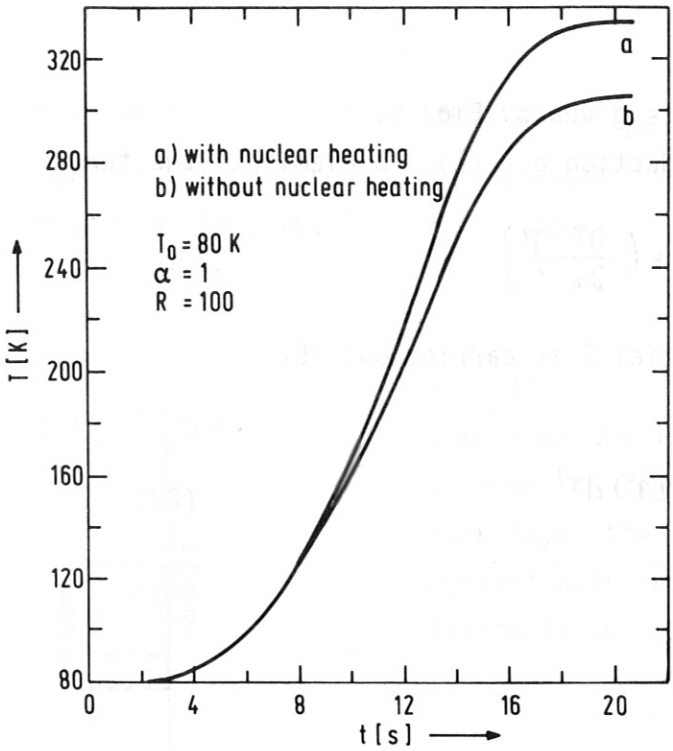

Fig. 9

Dependence of the conductor temperature at point A on pulse time with and without nuclear heating. The temperatures without nuclear heating are taken from Fig. 8.

Fig. 9 shows T versus t for a conductor located at A ($q = W_o$) with and without the influence of the nuclear energy deposition. The initial temperature T_o is 80 K. In this case the additional increase of T due to nuclear heating is about 28 K.

2.2 Temperature profiles in the electrical insulation layers

In this section the temperature profiles in the electrical insulation layers are investigated. Two insulation systems exist: the high-voltage insulation system and the interturn layer system. The high-voltage layer system is placed at the outer edges of the winding and protects the winding against electrical breakdown to ground. The temperature profiles are calculated for t = 13.5 s (end of flat top), where the components of the winding are most strongly influenced by forces. The temperature at the layer boundary are taken from the curves A in Fig. 8. The curves A in Fig. 8 show the strongest temperature increase perunit time and the highest T values of the whole coil. In this coil region the electrical insulation layers are therefore subjected to the largest temperature differences. For calculating the temperature profiles in the insulation layers we use the curves of Fig. 8, where the conductor temperatures are shown taking into account the magnetoresistance. The reason why we do not use the conductor temperature dependence shown in Fig, 9, where the nuclear heating is taken into account, is that the insulator is also homogeneously heated by the nuclear radiation by the same amount as the conductor ($\Delta T \approx 20$ K). The temperature difference between

conductor and insulator is therefore given by Fig. 8.
We start with the thermal heat conduction eq. (1). To eleminate the term

$$\frac{\partial \lambda}{\partial T}\left\{\left(\frac{\partial T}{\partial x}\right)^2+\left(\frac{\partial T}{\partial y}\right)^2+\left(\frac{\partial T}{\partial z}\right)^2\right\}$$

a transformation to the heat potential S is carried out /6/

$$S(T)=\frac{1}{\lambda_0}\int_{T_0}^{T}\lambda(T')\,dT' \tag{22}$$

where $\lambda_0 = \lambda(T = T_0)$.
Using the relations

$$\frac{\partial S}{\partial x}=\frac{\lambda}{\lambda_0}\cdot\frac{\partial T}{\partial x},$$
$$\frac{\partial^2 S}{\partial x^2}=\frac{1}{\lambda_0}\left[\frac{\partial T}{\partial x}\cdot\frac{\partial \lambda}{\partial x}+\lambda\frac{\partial^2 T}{\partial x^2}\right]\ etc. \tag{23}$$

The differential equation for the heat potential is now given by

$$\Delta S-\frac{1}{\kappa(S)}\cdot\frac{\partial S}{\partial t}+\frac{q}{\lambda_0}=0 \tag{24}$$

where the coefficient $\kappa(s)$ is defined by

$$\kappa(S)=\lambda(S)/\rho_m\cdot c(S) \tag{25}$$

Equation (24) has the same structure as the heat conduction equation (1) if $\partial\lambda/\partial T = 0$. The coefficient κ depends on S and via eq. (22) also on T. The temperature dependence of κ is only weak because λ (T) and c (T) show the same tendency in their temperature dependences. With decreasing temperature λ (T) and c (T) decrease. The weak temperature dependence of κ justifies the simplication of keeping κ constant when solving eq. (24).
A mean value $\bar{\kappa}$ is used which is defined as

$$\bar{\kappa}=[\kappa(T_0)+\kappa(T_{max})]/2 \tag{26}$$

$\kappa(T_0)$ being the value for the initial temperature T_0, and $\kappa(T_{max})$ the

κ-value for the maximum temperature T_{max} at 13.5s.

For the temperature profile calculations the following model is used (see Fig. 10). The insulation layer is infinitely extended in the z and y-directions.

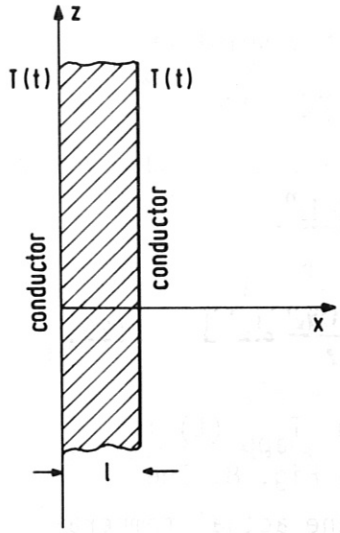

Fig. 10
Scheme of the insulation layer which is infinitely extended in the z and y-directions. For an inter-turn layer the insulator at x = 0 and x = l is in contact with the conductor. The high voltage insulation is in contact with the conductor at x = l.

Because the thickness l of the insulation layer is of the order of 1 mm whereas the extent in the other two directions is of the order of 1 m, this approximation of an infinitely extended sheet is justified.
Depending on the fact whether the insulation layer is an electrical interturn layer or the high voltage layer at the winding edge, the following boundary conditions are used:

$$T = f(t) \qquad \begin{matrix} x = 0 \\ x = l \end{matrix} \qquad (27a)$$

for the inter-turn layer and

$$T = f(t) \qquad x = l$$
$$\frac{\partial T}{\partial x} = 0 \qquad x = 0 \qquad (27b)$$

for the high-voltage insulation layer, which is heated only at x = l.
The condition $\partial T/\partial x = 0$ at x = 0 means that the heat flux is zero at x = 0.
The solution of eq. (24) with the symmetrical boundary condition (without the source term q) and for a temperature distribution $\varphi(x)$ in the layer at t = 0 is given by /6/

$$S(x,t) = \frac{2}{\ell} \sum_{n=1}^{\infty} e^{-\bar{\varkappa} n^2 \pi^2 t/\ell^2} \sin\frac{n\pi x}{\ell} \left[\int_0^{\ell} \varphi(x') \sin\frac{n\pi x'}{\ell} dx' + \right.$$

$$\left. + \frac{n\bar{\varkappa}\pi}{\ell} \int_0^{t} e^{\bar{\varkappa} n^2 \pi^2 t'/\ell^2} \cdot \left\{ f(t') - (-1)^n f(t') \right\} dt' \right] . \qquad (28)$$

For the assymmetrical boundary conditions (27) (q = 0) the solution reads /6/

$$S(x,t) = \frac{2}{\ell} \sum_{n=0}^{\infty} e^{-\bar{\varkappa}(2n+1)^2 \pi^2/4\ell^2} \cdot \cos\frac{(2n+1)\pi x}{2\ell} \left[\frac{(2n+1)\pi\bar{\varkappa}(-1)^n}{2\ell} \cdot \right.$$

$$\left. \cdot \int_0^{t} e^{\bar{\varkappa}(2n+1)^2 \pi^2 t'^2/4\ell^2} f(t')dt' + \int_0^{\ell} \varphi(x') \cdot \cos\frac{(2n+1)\pi x'}{2\ell} dx' \right] \qquad (29)$$

As boundary temperature function f (t) an approximation T_{app} (t) is used. The construction of the function T_{app} is shown in Fig. 8. The linear function T_{app} starts at t = 5 s and intersects the actual temperature function at $t = t_R + t_{FT}$ (13.5 s). T_{app} is given by

$$T_{app} = 80 + 18.588 \cdot t^* \qquad (30)$$

where t^* is (t-5) sec.

For carrying out the transformation to the heat potentials s the dependence of the thermal conductivity λ (T) on T has to be known. Figure A4 shows that the dependence of λ on T of the insulation to be used can be described by a linear function

$$\lambda(T) = \alpha + \beta T \quad . \qquad (31)$$

The linearized boundary function T_{app}

$$T_{app} = T_0 + k t^* \qquad (30')$$

is transformed according to (22) into

$$S(t^*) = \frac{k^2\beta}{2\lambda_0} t^{*2} + k t^* \quad . \qquad (32)$$

Inserting eq. (32) into eq. (28) yields the solution for S(x,t) with symmetrical boundary conditions

$$S(x,t^*) = \frac{k^2\beta}{2\lambda_0} t^{*2} + k t^* - \left[\frac{xl-x^2}{\bar{\varkappa}}\right]\left[\frac{k^2\beta}{2\lambda_0} t^* + \frac{k}{2}\right] + \frac{k^2\beta}{24\lambda_0\bar{\varkappa}^2}\cdot[xl-x^2]\cdot$$

$$\cdot[l^2+xl-x^2] - \frac{4k^2\beta l^4}{\lambda_0\bar{\varkappa}^2\pi^5}\sum_{n=0}^{\infty}\frac{e^{-\bar{\varkappa}(2n+1)^2\pi^2 t^*/l^2}}{(2n+1)^5}\cdot\sin\frac{(2n+1)\pi x}{\bar{\varkappa}\pi^3} +$$

$$+\frac{4kl^2}{\bar{\varkappa}\pi^3}\sum_{n=0}^{\infty}\frac{e^{-\bar{\varkappa}(2n+1)^2\pi^2 t^*/l^2}}{(2n+1)^3}\cdot\sin\frac{(2n+1)\pi x}{l} \quad . \tag{33}$$

The back-transformation from S to T is given by

$$T = \frac{1}{\beta}\left\{[2\beta(\lambda_0 S+\gamma)+\alpha^2]^{1/2} - \alpha\right\} \tag{34}$$

with

$$\gamma = \alpha T_0 + \frac{\beta}{2}T_0^2 \quad . \tag{35}$$

For deriving formula (33) the following relations were used:

$$\sum_{n=0}^{\infty}\frac{1}{(2n+1)}\cdot\sin\frac{(2n+1)\pi x}{l} = \pi/4 \quad ,$$

$$\sum_{n=0}^{\infty}\frac{1}{(2n+1)^3}\cdot\sin\frac{(2n+1)\pi x}{l} = \frac{\pi^3}{8}\cdot\frac{x}{l}(1-x/l) \quad , \tag{36}$$

$$\sum_{n=0}^{\infty}\frac{1}{(2n+1)^5}\cdot\sin\frac{(2n+1)\pi x}{l} = \frac{\pi^5}{96}\cdot\frac{x}{l}(1-x/l)(1+x/l-x^2/l^2) \quad .$$

For the asymmetric boundary conditions (27b) the solution for S is given by

$$S(x,t^*) = \frac{k^2\beta t^{*2}}{2\lambda_0} + k t^* - \frac{[l^2-x^2]}{\bar{\varkappa}}\left[\frac{k^2\beta}{2\lambda_0} t^* + \frac{k}{2}\right] + \frac{k^2\beta l^4}{12\bar{\varkappa}^2\lambda_0}\cdot$$

$$\cdot\left[\frac{x^4}{2l^4} - \frac{3x^2}{l^2} + \frac{5}{2}\right] - \frac{128\,l^4}{\bar{\varkappa}^2\pi^5}\sum_{n=0}^{\infty}\frac{(-1)^n e^{-\bar{\varkappa}(2n+1)^2\pi^2 t^*/4l^2}}{(2n+1)^5}\cdot \tag{37}$$

$$\cdot\cos\frac{(2n+1)\pi x}{2l} + \frac{16\,l^2}{\bar{\varkappa}\pi^3}\sum_{n=0}^{\infty}\frac{(-1)^n e^{-\bar{\varkappa}(2n+1)^2\pi^2 t^*/4l^2}}{(2n+1)^3}\cdot\cos\frac{(2n+1)\pi x}{2l} \quad .$$

Relation 37 can also derived from eq. (33) by carrying out a transformation of the centre of the layer and by substituting 2l for l.

For insulation layers heated symmetrically at both boundaries (x = 0, x = l) temperature profiles are shown in Fig. 11. The thickness l of the layers varied from 0.06 cm to 1 cm. The profiles are calculated for the end of the flat-top phase ($t = t_R + t_{FT}$). During the flat-top phase the highest load to the coil occurs at the end of this phase because then the highest temperature

coincides with the full magnetic forces.
For calculating the temperature profiles the following material relations and data were used (see Fig. A4 und A5). The linearized thermal conductivity λ (T) is given by

$$\lambda(T) = 9 \cdot 10^{-4} + 5.83 \cdot 10^{-6} T \quad , \tag{38}$$

and the mean value of $\varkappa$, $\bar{\varkappa} = 1.64 \times 10^{-3}$ ($cm^2 s^{-1}$).
The temperature profiles shown in Fig. 11 calculated with rel. (33) are identical with the profiles for a high-voltage insulation layer [boundary conditions (27)], which are only half as thick as the inter-turn layers.

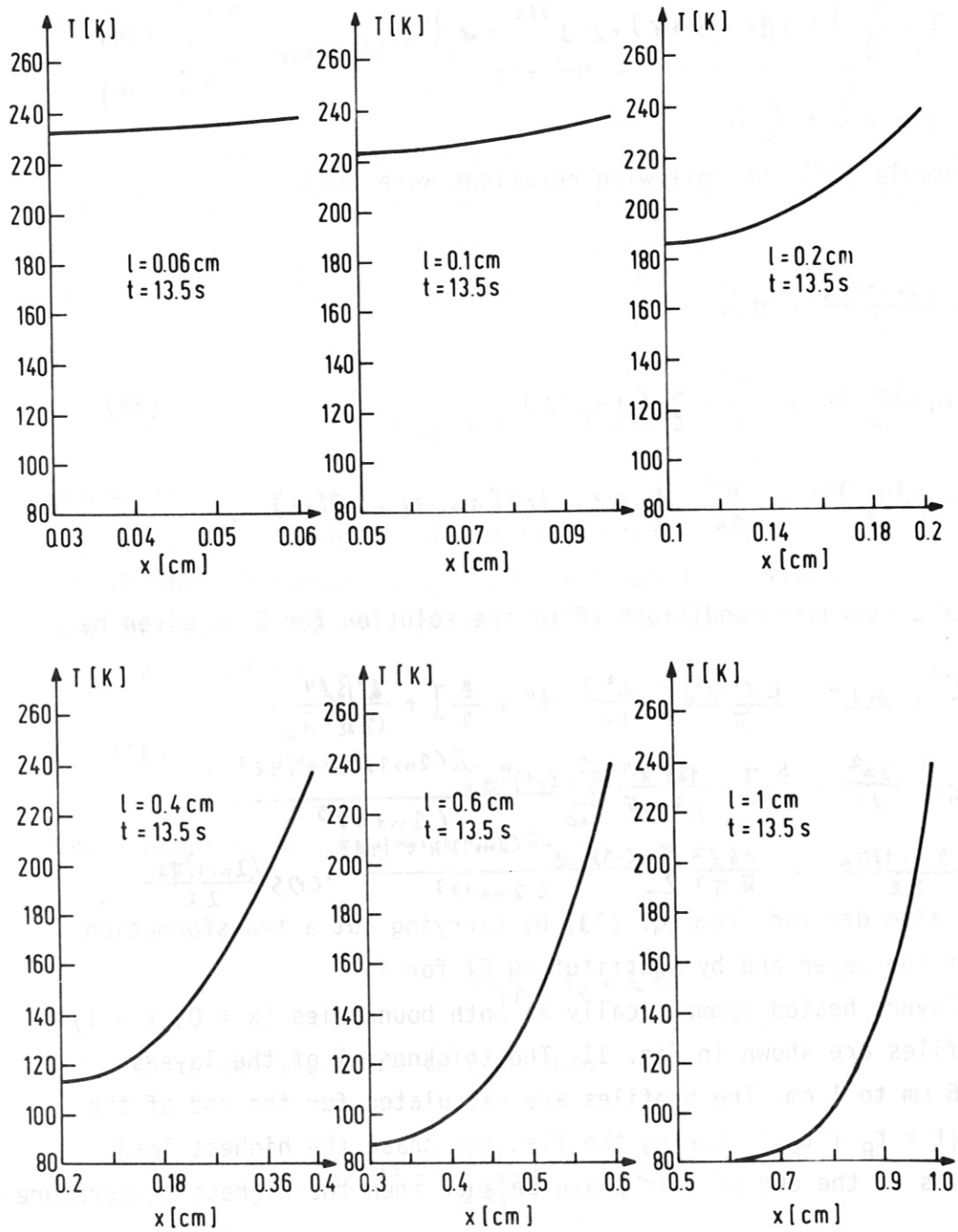

Fig. 11
Temperatur-profiles in inter-turn insulation layers for LN_2-cooled coils (T_o = 80) at the end of the flat-top phase (t^* = 8.5s, t = 13.5 s). (Only one half of the layer is shown because the temperature are symmetric to the middle plane)

3. Numerical calculations

As described in Sec. 2, analytical calculations can only be carried out by making symplyfying assumptions. The material function f, for instance, was approximated by a linear function of the temperature. To omit such approximation mimerical calculations were made.

3.1. Description of the TEVBA computer code

With the TEVBA computer code the temperatures and the ohmic heating losses of the tape-wound toroidal coil system can be calculated. The abbreviation TEVBA stands for the German words, Temperatur und Verlust für Bandspulen-systeme (temperature and loss for tape-wound coil systems).
The computer program is based on eq. (3) - neglecting the thermal conduction - and reads

$$\rho_m c \cdot \frac{\partial T}{\partial t} = \rho_e j(t) + q \tag{3'}$$

where $\rho_m \cdot c$ is the specific heat (in J/m^3k), ρ_e = the specific resistivity, j = the current density and q = the nuclear energy deposited in the winding; $\rho_m \cdot c$, and ρ_e are temperature-dependent, j and q are time-dependent.
The specific resistivity is composed of three parts, the residual resistivity ρ_{eo}, which depends on the degree of the imperities of the copper, the "phonon term" ρ_{eP} (T) and the magnetoresistance ρ_{eB} :

$$\rho_e = \rho_{eo} + \rho_{eP}(T) + \rho_{eB} \tag{2}$$

The residual resistivity ρ_{eo} of copper can be described by the residual resistivity ratio $R = \rho_e(300)/\rho_e(4.2)$ in the following way:

$$\rho_{eo} = \frac{2 \times 10^{-9}}{R} \quad [\Omega m]. \tag{39}$$

The "phonon term" ρ_{eP} (T) was fitted by a polynamical of the seventh order

$$\rho_{eP}(T) = \sum_{n=0}^{7} b_n T^n \tag{40}$$

The specific heat fuctions of copper and steel (see Fig. A3) are also fitted by polynamicals of the seventh order

$$c_c = \sum_{n=0}^{7} a_{cn} T^n \quad , \quad c_s = \sum_{n=0}^{7} a_{sn} T^n \qquad [J/kgK] \tag{41}$$

where c stand for copper and s for stainless steel. The coefficients b_n, a_{cn}, a_{sn} are summarized in Table II.

n	a_{cn}	a_{sn}	b_n
o	1.268	1.9667	4.7228×10^{-12}
1	-1.2938	-1.4177	1.3337×10^{-12}
2	9.7959×10^{-2}	1.3615×10^{-1}	-4.167×10^{-13}
3	-6.879×10^{-4}	-1.8821×10^{-3}	2.0006×10^{-14}
4	-6.9413×10^{-7}	1.3328×10^{-5}	-2.0208×10^{-16}
5	2.4101×10^{-8}	-5.2093×10^{-8}	9.7319×10^{-19}
6	9.0142×10^{-4}	1.0588×10^{-10}	-2.3290×10^{-21}
7	1.0648×10^{-13}	-8.7257×10^{-14}	2.2121×10^{-24}

Table II: Coefficients for the specific heat of copper (a_{cn}), for stainless steel 310SS (a_{sn}) and for the specific resistivity of copper (b_n).

For the specific masses of copper and stainless steel the values $8.9 \times 10^3 kg/m^3$ and $7.9 \times 10^3 kg/m^3$, respectively, were used.

The accuracy of the polynomal fit is shown in Table III, where the c_C, c_S and ρ_e-values at the reference points taken from the figures A1 and A3 are compared with the corresponding values yielded by the polynomicals, which were derived using the least squares fit technique.

As can be seen from Table III, the specific heat data are well approximated by the polynamicals for temperatures $T > 10K$. The "phonon term" of the specific resistivity ρ_e is only well approximated for temperatures $T < 20K$. Because the residual resistivity R of the copper material used in magnet design is 100 about a factor of as large (see A1) as the ρ_{eP} values below 20K, this inaccuracy has no noticeable influence on the calculation.

The magnetoresistance term for copper (see A2) is given (in linearized form) by

$$\rho_{eB} = a \cdot B \quad . \tag{41}$$

The numerical value of a is 5×10^{-11} $\Omega m/T$.

X (I)	Y (I)	YP (I)	
0.0	0.0	1.96671D+00	
1.00000E+01	5.00000E+00	-3.49457D-01	
2.00000E+01	1.20000E+01	1.49879D+01	
4.00000E+01	6.90000E+01	7.18477D+01	
6.00000E+01	1.40000E+02	1.37425D+02	
8.00000E+01	2.00000E+02	1.97400D+02	
1.00000E+02	2.45000E+02	2.48576D+02	specific heat of stainless steel S310
1.50000E+02	3.50000E+02	3.49814D+02	
2.00000E+02	4.21000E+02	4.21415D+02	
2.50000E+02	4.62000E+02	4.61902D+02	
3.00000E+02	4.85000E+02	4.84937D+02	
0.0	0.0	1.26822D+00	
1.00000E+01	1.00000E+00	-2.56553D+00	
2.00000E+01	7.00000E+00	9.03843D+00	
4.00000E+01	6.00000E+01	6.26041D+01	
6.00000E+01	1.38000E+02	1.33676D+02	specific heat
8.00000E+01	2.00000E+02	2.01956D+02	of copper
1.00000E+02	2.56000E+02	2.56292D+02	
1.50000E+02	3.26000E+02	3.25602D+02	
2.00000E+02	3.58000E+02	3.58165D+02	
2.50000E+02	3.78000E+02	3.77952D+02	
3.00000E+02	3.90000E+02	3.90008D+02	
0.0	1.00000E-14	4.72282D-12	
1.00000E+01	5.00000E-13	-5.52890D-12	
2.00000E+01	8.00000E-12	-4.59503D-12	
4.00000E+01	2.00000E-10	2.44915D-10	specific
6.00000E+01	1.00000E-09	9.41313D-10	resistivity
8.00000E+01	2.00000E-09	2.03533D-09	of copper
1.00000E+02	3.40000E-09	3.39333D-09	("phonon term")
1.50000E+02	7.20000E-09	7.19830D-09	
2.00000E+02	1.10000E-08	1.10008D-08	
2.50000E+02	1.43000E-08	1.42995D-08	
3.00000E+02	1.70000E-08	1.69993D-08	

Table III Comparison between the material data at the temperature [I] taken from the curves A1 and A3 Y [I] and calculated with the polynomials YP [I]

The numerical calculations are carried out using a finite element subdivision of the coil. In Fig. 12a the finite element subdivision used for the following calculations is shown. The coil is subdivided into 3-dimensional isoparametric volume elements with 20 nodal points (for a description of this element see /8/). For each nodal point the temperature T and for each element the ohmic heating losses p_t are calculated.

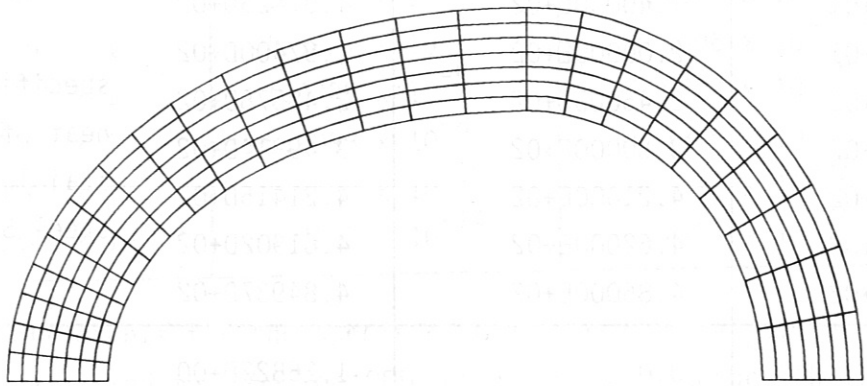

Fig. 12a Subdivision of a half-torus magnet into elements. The number of elements is 336 and the number of nodal points 2101.

The principal calculation process is as follows:

a) Calculation of the current density j for each nodal point. The current density j is given by

$$j = j_0 \begin{cases} t/t_R & 0 \le t \le t_R \\ 1 & t_R < t \le t_R + t_{FT} \\ 1 - \dfrac{t - t_{FT} - t_R}{t_D} & t_R + t_{FT} < t \le t_R + t_{FT} + t_D \end{cases}, \qquad (42)$$

where j_0 depends on the x-coordinate of the nodal point x (see relations (9) and (10)).

b) Calculation of the magnetoresistance term $\rho_{eB} = a \cdot B$.
The magnetic induction B at the inner edge of the coil for the plane i (see Fig. 12b) is given by

$$B_i = \frac{\mu_0 I_g}{2\pi x_i} \qquad (43)$$

For nodal points which are located at a distance δ from the inner edge, the magnetic induction value is calculated from

$$B = B_i [1 - \delta/D], \qquad (44)$$

which means that a linear decrease of B over the winding is assumed.

c) Calculation of the nuclear heating term q

The nuclear heating term is given by

$$q_{n,\gamma} = W_0 \, e^{-\lambda' \delta} \qquad x \leq x_G$$

$$q_{n,\gamma} = W_0 \, e^{-\lambda'(\delta + d)} \, (1 - \delta / 1.1 D)^{1/2} \qquad x > x_G \tag{45}$$

where d is the thickness of the flange which supports the coil for $x > x_G$.

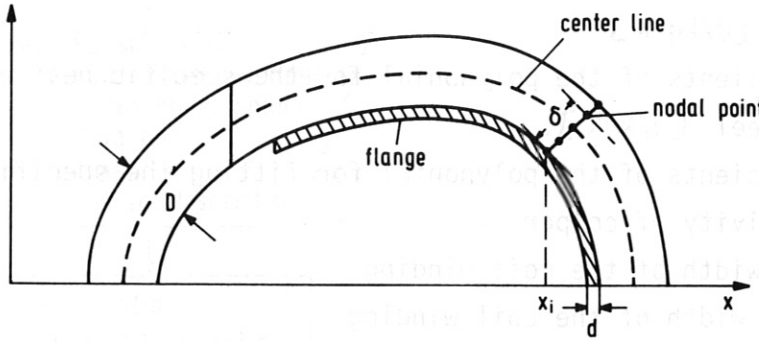

Fig. 12b Scheme of the coil with the plane i havig 5 nodal points

For calculation of both B and q, the distance δ has to be determined. For this purpose the nodal points located in the plane i have to be known.

d) Calculation of the temperature

Equation (3') is solved for each nodal point.

e) Calculation of the ohmic heating losses

The ohmic heating losses are calculated for each element.

The losses are given by

$$P = \rho_e(TM) \cdot j^2 \cdot V_{cu} \tag{46}$$

(TM = mean temperature of the element considered and V_{cu} = copper volume of the element); V_{cu} is given by

$$V_{cu} = V_0 \cdot T' \quad , \tag{47}$$

where Γ is the filling factor, given by

$$\Gamma = \begin{cases} \dfrac{[B-\Delta B][D-\Delta D]}{B\cdot D[1+\alpha]} & x > x_s \\ \dfrac{[2x_M\cdot\tan(\pi/n)-\Delta B][D-\Delta D]}{2x_M\cdot\tan(\pi/n)\cdot D[1+\alpha]} & x < x_s \end{cases} \qquad (48)$$

(ΔB and ΔD are defined by eqs. (11) and (12)).

The input data for TEVBA are:

AC(N)	coefficients of the polynonial for the specific heat of copper [J/kg K]
AS(N)	coefficients of the polynonial for the specific heat of the steel [J/kgK].
BW(N)	coefficients of the polynonial for fitting the specific resistivity of copper
BAX	axial width of the coil winding
BRA	radial width of the coil winding
DEL	distance of the nodal point from the coil inner edge
DELTA	thickness of the flange
DERY	error parameter for RUNGE-KUTTA
DHIS	thickness of the high-voltage insulation
DLIS	thickness of the layer insulation
DSPL	thickness of the spacer plate; for hollow-conductor cooling DSPL = F1 x NK/BRA, where F1 is the cross-sectional area and NK is the number of hollow conductor
FABB	coefficient of the magnetoresistance term [Ωm/T]
FL	nuclear absorption coefficient (reciprocal of the mean freepath)
NC	number of coefficients
NDIM	
NLSP	number of layers per coil
NSP	number of coils
NSW	= 0 without nuclear heating (Q = 0) = 1 with nuclear heating
NxM	number of nodal points
R	residual resistivity ratio
RHOO	specific resistivity of copper at room temperature
STR	total ampere-turns of the torus
TD	shut-down time
TF	flat-top time

TR	rise time
TTO	start temperature (temperature at the beginning of the current pulse)
WO	nuclear heat deposition at the inner coil edge
XG	x coordinate at the beginning of the flange
XS	tapering edge.

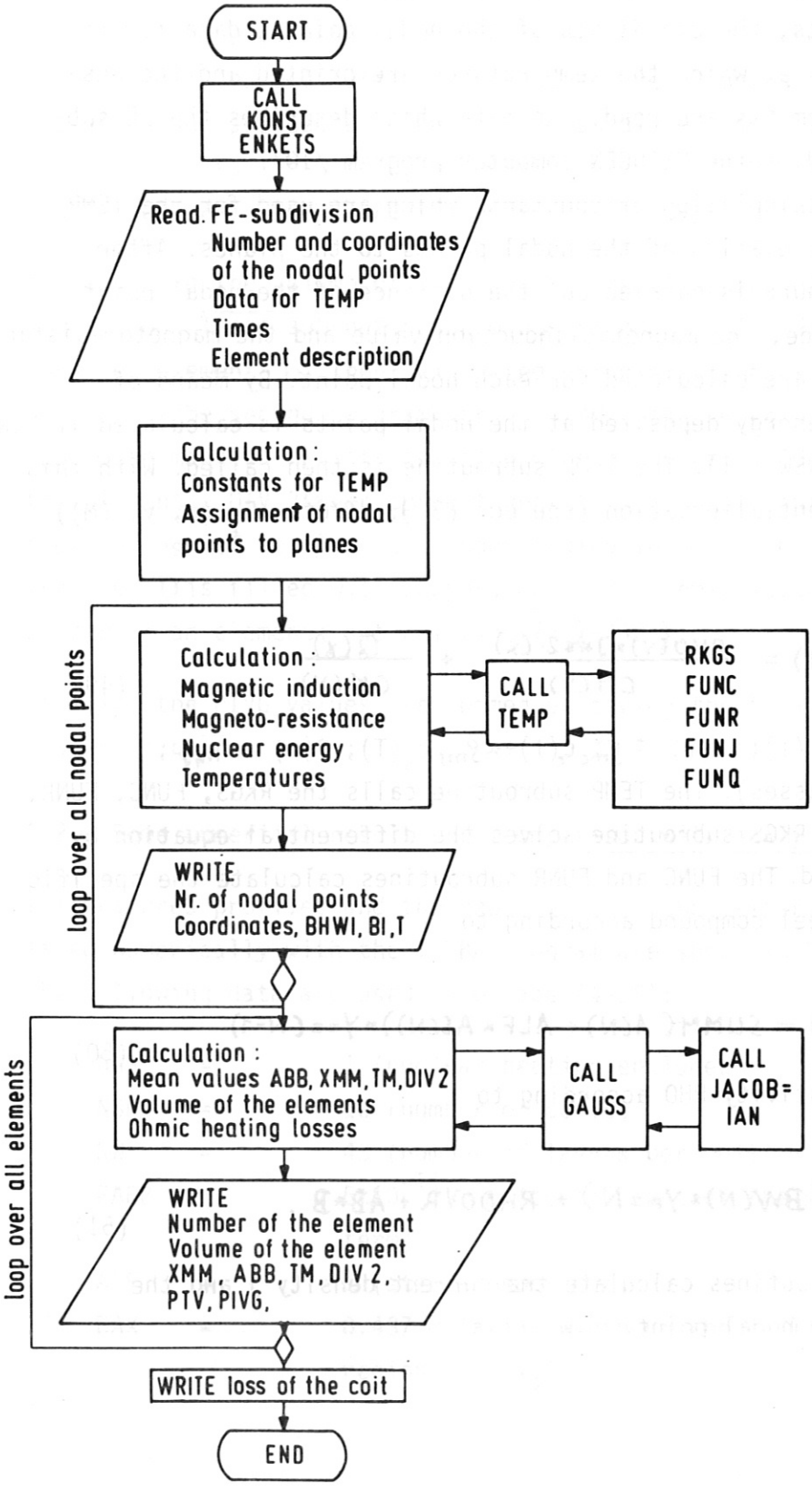

Fig. 13

Structure of the TEVBA computer program

The structure of the TEVBA program is shown in Fig. 13. At the beginning of the calculation the subroutines KONST and ENKETS are called. The KONST subroutine contains the coefficients collected in Table II. The ENKETZ subroutine /9/ is used for calculating the shape functions /8,9/ and their derivatives at the mesh points.
The finite-element subdivision, (given by the numbers NK, NR, NS), the numbers of nodal points, the coordinats of the nodal points, data for the TEMP subroutine, times at which the temperatures are printed and the description of the FE elements are read. The data which describes the FE subdivision is calculated by the MESHGEN computer program /10/.
The next step is the calculation of constants which are used for the TEMP subroutine and the correlation of the nodal points to the planes. After the correlation procedure is carried out the distance of the nodal point from the coil inner edge, the magnetic induction value and the magnetoresistance according to eq. (41) are calculated for each nodal point. By means of eq. (45) the nuclear energy deposited at the nodal points is calculated if NSW is set equal to one (NSW = 1). The TEMP subroutine is then called. With this subroutine the differential equation (see eq. (3 '); $dT/dt = F_1(x, y, (M))$

$$F1(X,Y,CM) = \frac{RHO(Y)*J**2(X)}{CM(Y)} + \frac{Q(X)}{CM(Y)} \qquad (49)$$

is solved (RHO(Y) ≡ (T); CM(Y) ≡ $\varrho_{mc} c_c(T) + \alpha \varrho_{ms} c_s(T)$; Q(x) = $q_{n,\gamma}$; ϱ_m are the specific masses). The TEMP subroutine calls the RKGS, FUNC, FUNR, RUNJ subroutines. The RKGS subroutine solves the differential equation by the Runge-Kutta-method. The FUNC and FUNR subroutines calculate the specific heat of the copper-steel compound according to

$$CM(Y) = SUMM(A(N) + ALF*AS(N))*Y**(N-1) \qquad (50)$$

and the specific resistivity RHO according to

$$RHO = (BW(N)*Y**N) + RHOO/R + AB*B\,. \qquad (51)$$

The FUNJ and FUNQ subroutines calculate the current density j and the nuclear heating at the nodal point.

The computer program continues by writing the number of nodal points, the magnetic induction value BHWI at the inner edge of each plane to which the nodal point is correlated, the magnetic induction value of the nodal point BI and the temperature T. The second part of the TEVBA program is concerned with the calculation of the ohmic heating losses. For each element the mean values of T, XM, DIV2 and AB are calculated. The average procedure covers the twenty nodal points of each element. To get sufficently accurate results (as a consequence of the averaging procedure), the coil is subdivided into a fine mesh (see Fig. 12a)across the winding where the strongest variations (T,B and q) ocurr . DIV 2 is the current density in the tapered region of the coil.

To calculate the volume of an element, the GAUSS and JACOBIAN subroutine are called. These subroutines are described in Ref. /9/. The ohmic heating loss per element is then calculated using eqs. (46) - (48). The output data from the second program part is XMM (mean XM value of the element), ABB (mean magneto-resistance value of the element), TM (mean T value of the element), DIV 2(mean current density of the element), PTV (ohmic heating loss of an element without taking into account that only the fraction η is filled with copper) and PTVG (ohmic losses produced in the copper of an element; see relations (46)-(48)).

Finally, the PIVG values are summed up giving the total ohmic heating losses of half a coil.

3.2. Some numerical results and comparison with analytical calculations

Temperatures profiles and the dependence of the temperature on time calculated numerically with the TEVBA program are shown in Figs. 14 - 18. The following data are used (see page 24-25):

NWS	=	1 (nuclear heating encluded)
NSP	=	16 (number of coils)
NW	=	43 (number of layers per coil)
FABB	=	$5 \times 10^{-11}\ \Omega \cdot m$ (coefficient of the magneto-resistance term)
ALF	=	1 (steel-copper ratio)
BAX	=	0.437 m (axial width of the coil in parallel flank region ($x > x_s$))

BRA	=	0.435 m (radial width of the coil; D in fig.1)
WO	=	12.7×10^6 w/m^3 (nuclear heating at the inner coil edge)
DHIS	=	0.003 m (thickness of the high-voltage insulation; Δl_H in rel. (11))
DLIS	=	0.004 m (thickness of the inter-term insulation; l_S, in rel. (12)
DSPL	=	0.006 m (thickness of the spacer plate)
FL	=	9.68 m^{-1} (nuclear absorption coefficient)
R	=	100 (resudual resistivity ratio)
RHCO	=	1.7×10^{-8} Ωm (resistivity of copper at room temperature)
STR	=	61.7 MA (total current of the TF system)
DELTA	=	0.1 or 0.05 m (thickness of flange)
TR	=	7 s (current rise time) } see Fig. 2
TF	=	6.5 s (flat-top time) } see Fig. 2
TD	=	7 s (shut-down time) } see Fig. 2
TTO	=	30-80 K (stark temperature T_o)
XG	=	1.1 m (x coordinate of the beginning of the flange)
XS	=	1.1 m (x coordinate of the tapering edge)

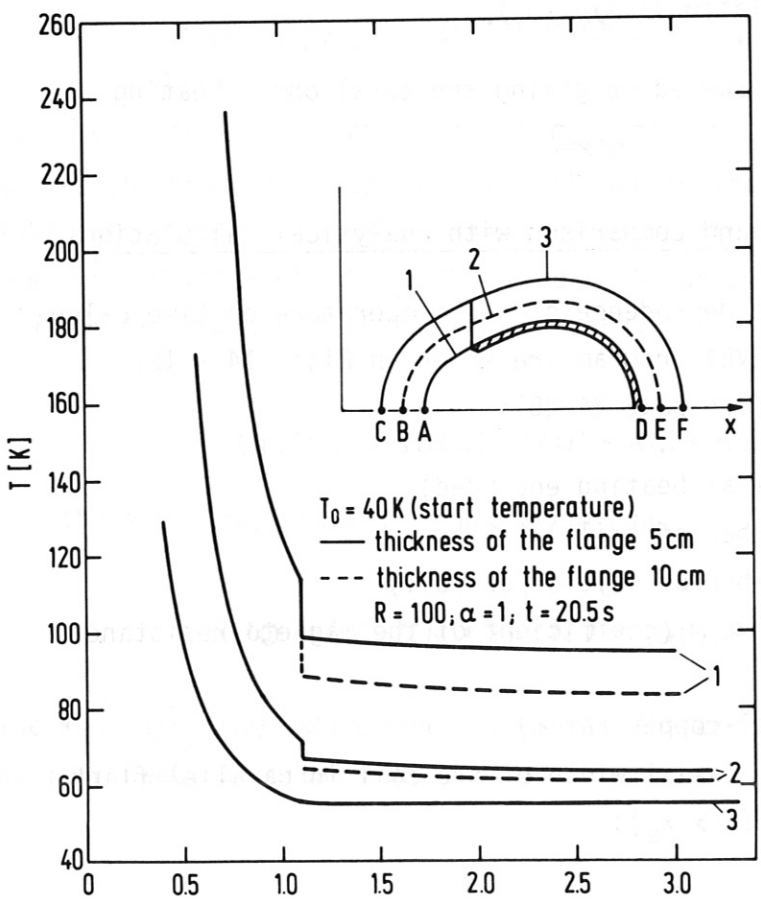

Fig. 14

Temperature profile at the end of the current pulse (t = 20.5 s) for an initial temperature T_o = 40 K

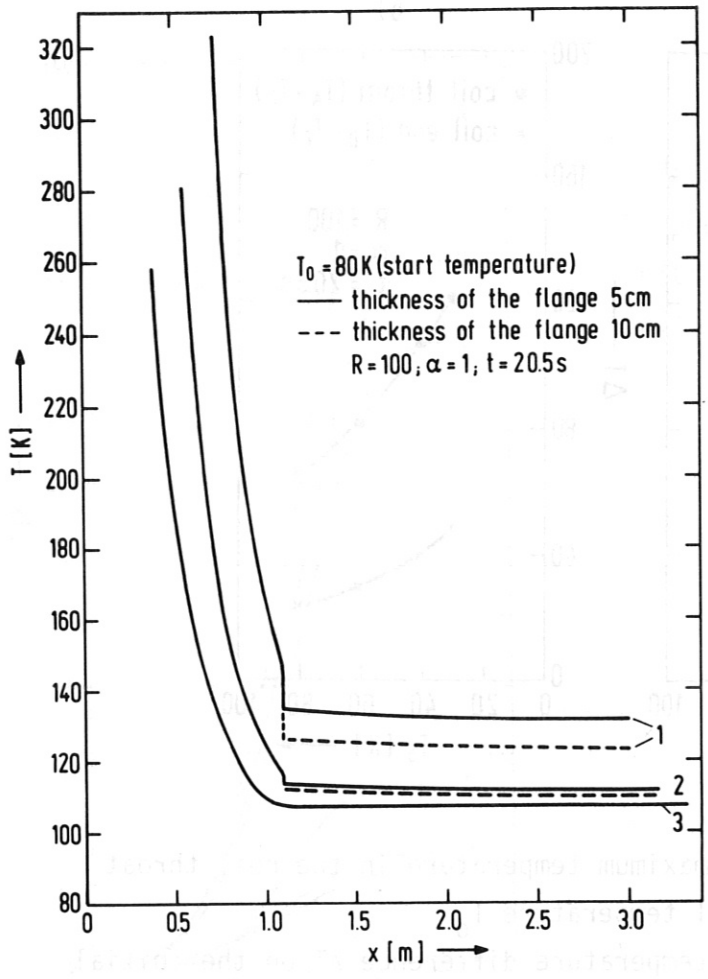

Fig. 15
Temperature profile at the end of the current pulse (t = 20.5 s) for an initial temperature T_o = 80 K.

In Figs. 14 and 15 the temperatures along the inner edge, the centre line and the outer edge (curves 1, 2 and 3) for coil with an initial temperature T_o = 40 and 80 K are shown. The temperature jump at x = 1.1 m is produced by the flange. The jump of the temperature at x = 1.1 m is governed by the thickness of the flange. Although the current density is constant across the coil winding area, there are large temperature differences between the inner and outher edges. They are produced by the enhanced resistivity at the inner edge due to the magneto-resistance and by the nuclear heating, which decrease exponentially across the winding.

With decreasing initial temperature T_o the temperature difference ΔT increases as shown in Fig. 16b, because the influence of the magneto-resistance and the nuclear heating increases. The maximum temperature T_{max} (temperature at point A for t = 20.5s) strongly decreases with decreasing T_o (see Fig. 16a). The temperature rise of a conductor at the locations A, B, C, D, E, F with an initial temperature of 40 K and 80 V is shown in Figs. 17 and 18.

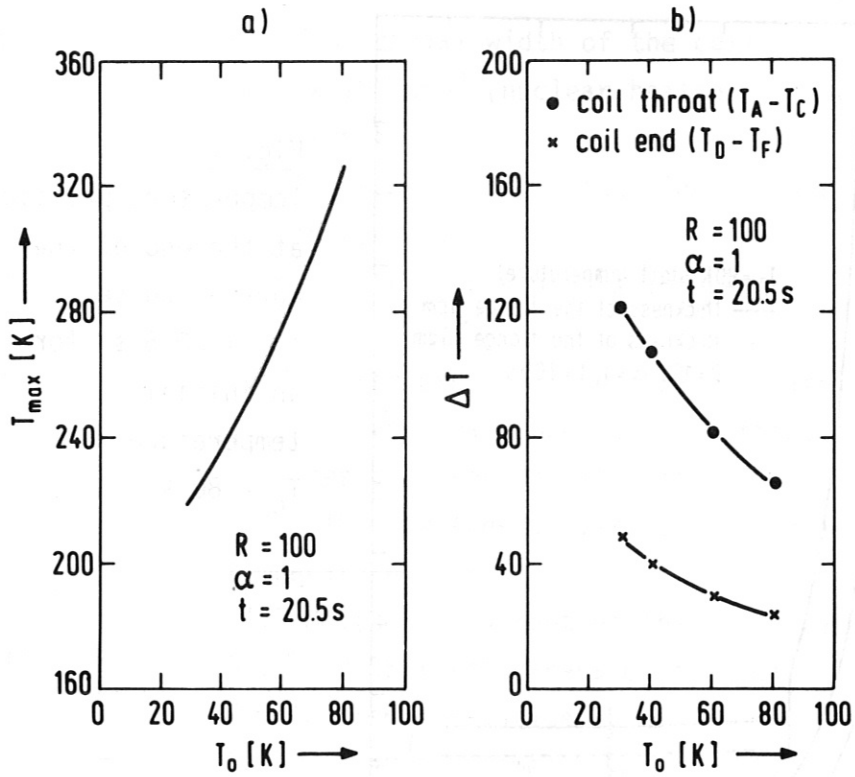

Fig. 16 a) Dependence of the maximum temperature in the coil throat T_{max} on the initial temperature T_o

b) Dependence of the temperature difference ΔT on the initial temperature T_o.

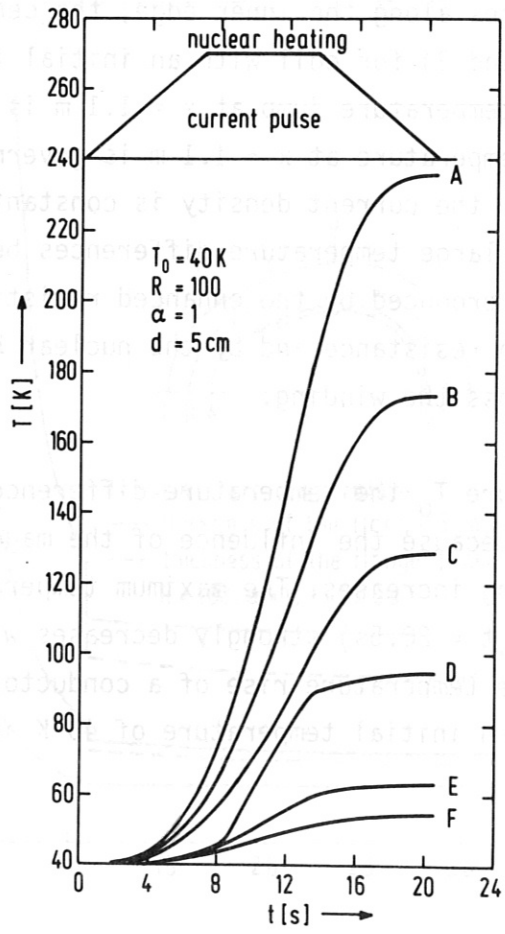

Fig. 17

Temperature rise versus time for an initial temperature of 40 K (nuclear heating is included)

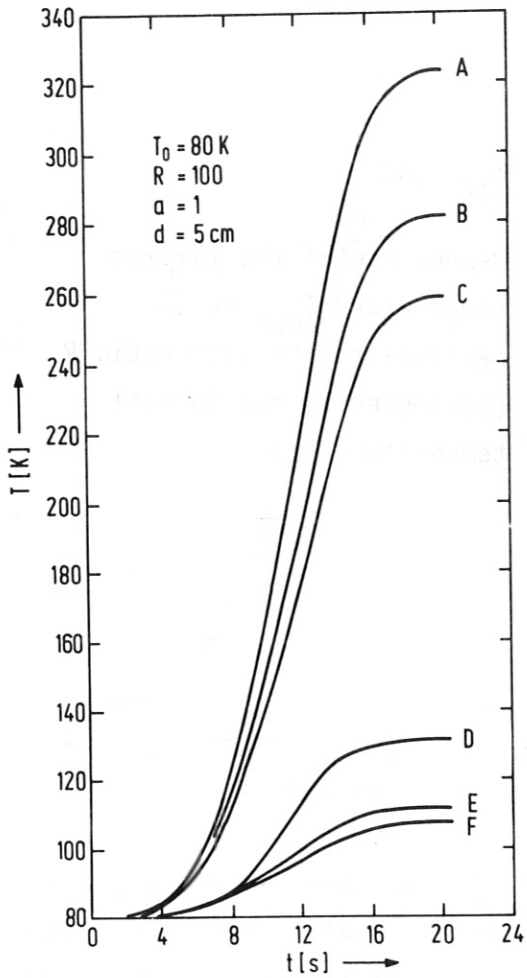

Fig. 18

Temperature rise for an initial temperature of 80 K (nuclear heating is included)

The results of Figs. 14 - 18 were calculated with a residual resistivity ratio R = 100. This value is characteristic of commercial copper . The influence of R on the maximum temperature T_{max} and ΔT in the coil throat are shown in Figs. 19 and 20. With decreasing R the maximum temperature increases; the temperature difference ΔT across the winding in the coil throut decreases with decreasing R (increasing defect concentration). Both figures show that the influence of R increases with decreasing initial temperature T_0.
In Fig. 21 numerically and analytically calculated T values are compared. The curves correspond to temperatures of a conductor at point A with nuclear heating. The difference in the maximum temperature at the end of the current pulse is 2,8 %.

In designing a toroidal magnet system the ohmic losses and the total energy due to the ohmic losses deposited in the system during the current pulse are important parameters.

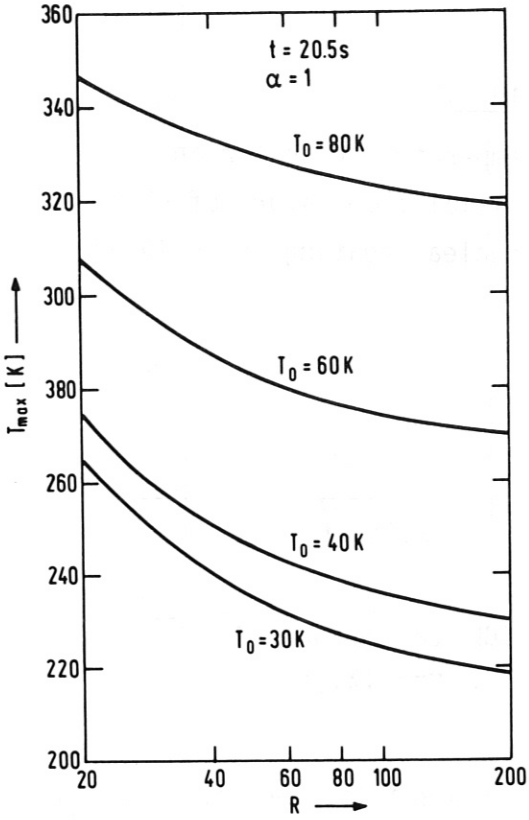

Fig. 19

Dependence of the maximum temperature T_{max} on the residual resistivity ratio R (parameter is the initial temperature T_o).

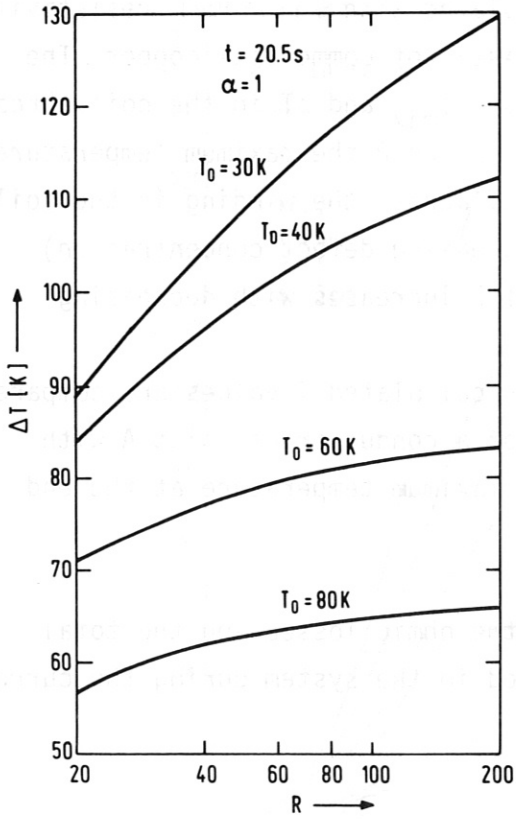

Fig. 20

Dependence of the temperature difference ΔT across the winding in the coil throat (T_A - T_C) on the residual resistivity ratio R.

T_A = temperature at point A

T_C = temperature at point C

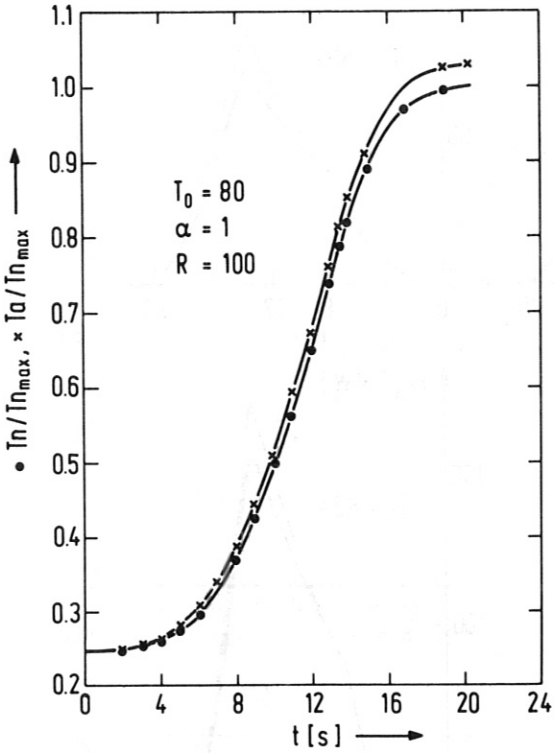

Fig. 21

Comparison of analytically and numerically calculated temperatures. The curve labelled • corresponds to curve A of Fig. 18, normalized to the maximum temperature T_{nmax} (T_n and T_a stands respectively for numerically and analytically calculated temperatures); the curve labelled x corresponds to curve a of Fig. 9.

The dependence of the ohmic losses on the time are shown in Fig. 22. The initial temperature varies between 30 and 80 K. As a consequence of the large increase of the electrical resistivity the ohmic heat losses strongly depend on the initial temperature. For the results of Fig. 22 the flange thickness is 10 cm. The maximum electric power for compensating the ohmic losses as about 170 MW for a liquid-N_2-cooled system (T_o = 80 K).

The energy deposited in the TF system produced by ohmic heating is given by

$$E_{OH} = \int_0^{20.5} P_{OH}\,dt \qquad (52)$$

The energy E_{OH} has to be cooled away in the time interval (pulse cooling time) between two pulses. A pulse cooling time of 1 h is envisaged. As Fig. 23 shows, the energy E_{OH} strongly decreases with T_o. Reducing T_o from 80 K to 40 K produces a reduction of E_{OH}-from 1.37 GJ to 0.43 GJ ($\sim$ 30 %).

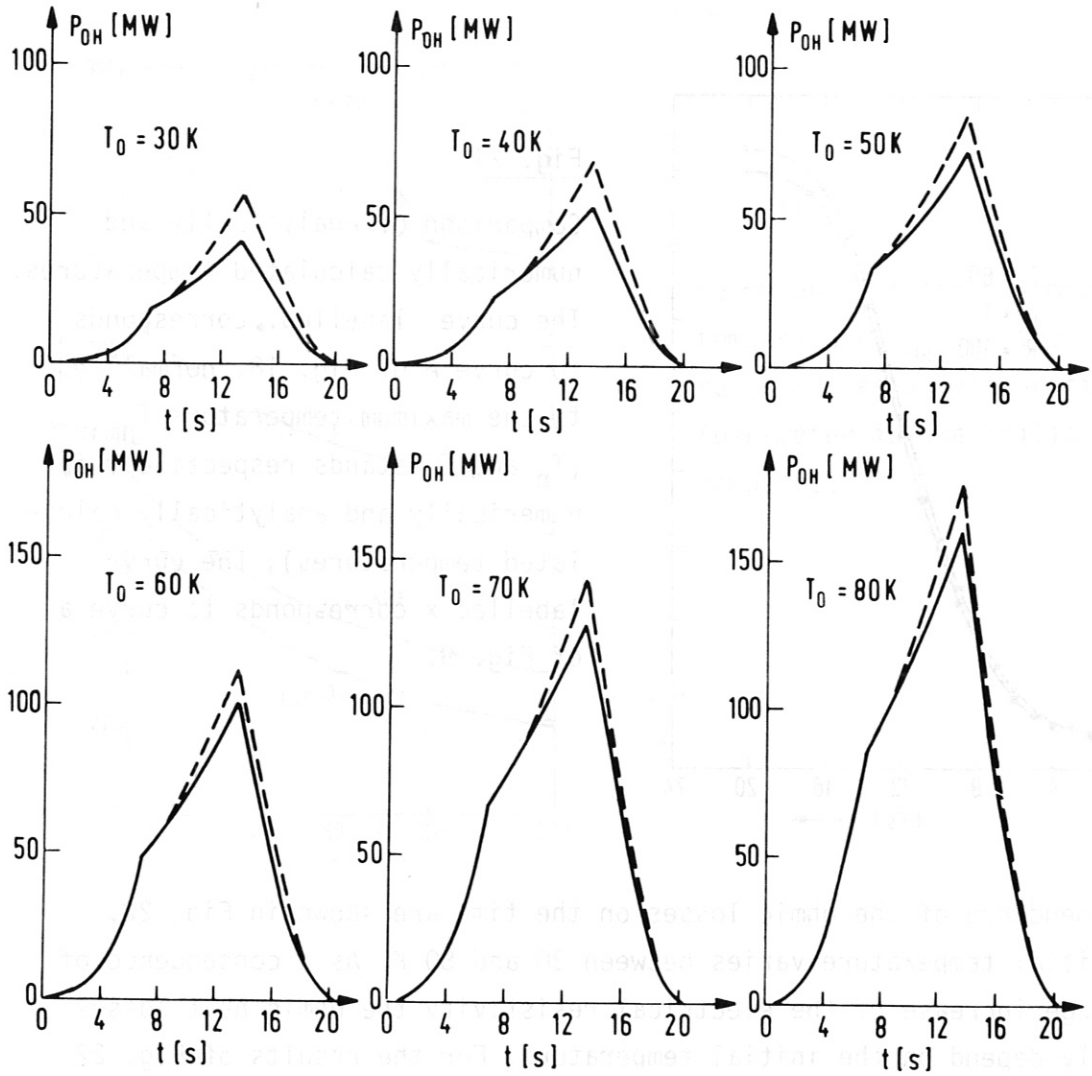

Fig. 22 Ohmic heating losses for the TF coil system during the current cycle. The initial temperature T_0 varies from 30 K to 80 K. The losses are calculated with (-) and without (--) nuclear heating; the resistivity ratio R = 100, the steel copper ratio α = 1 and the flange thickness d = 0.1 m (see Fig. 12b)

The electric power necessary for cooling the TF coil system during 1 h depends on the energy deposited in the coil winding and on the efficiency of the refrigeration system. The efficiency is characterized by the ratio P_e/P_c, where P_e stands for the electric power and P_c stands for the power "cooled away" at cryogenic temperature T_o. P_c is given in our study by $P_c = E/3600$, where E is the energy deposited in the magnet system. The ratio P_e/P_c is given by

$$P_e/P_c = 5.05 \cdot 10^3 \cdot T_o^{-1.4}$$

(see figure on page 6 of Ref. /4/).

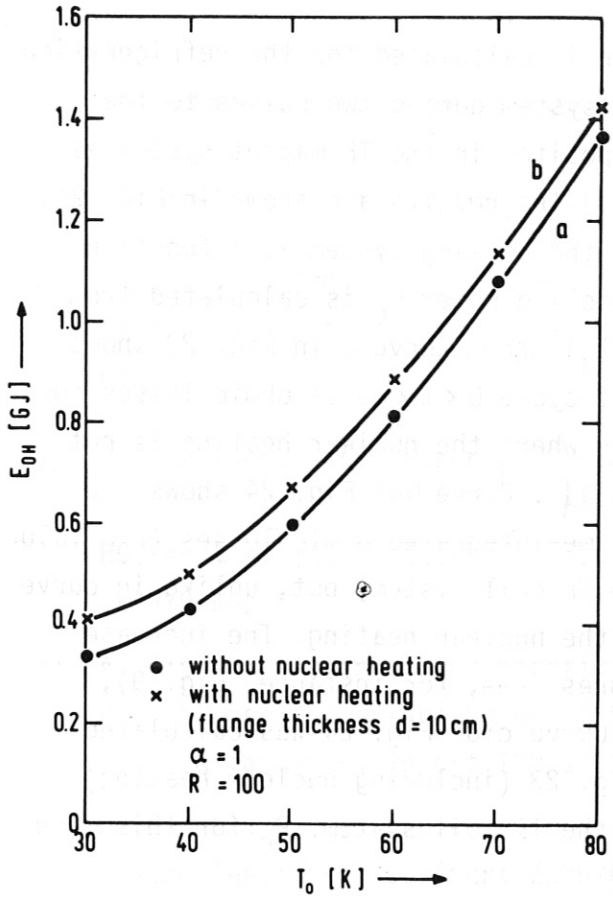

Fig. 23

Total ohmic heating energy deposited in the TF coil system after the current cycle versus the initial temperature T_o.

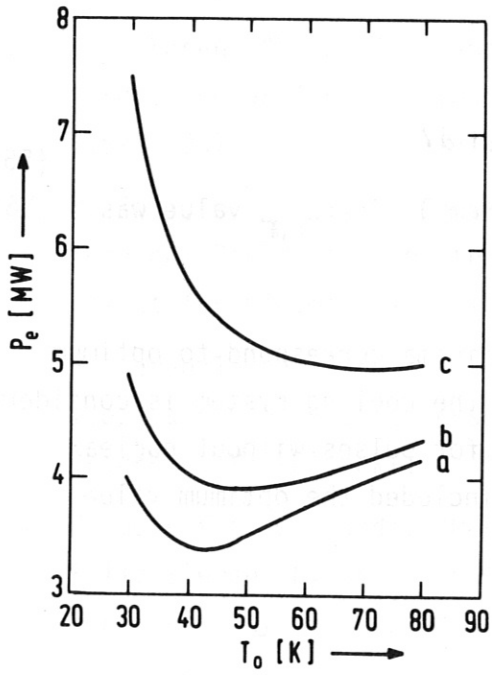

Fig. 24

Electric power P_e for the refrigerator, for cooling the TF coil system, versus the initial temperature T_o. Cooling time one hour.
In the curves a and b only the ohmic losses $\rho_e j^2$ are considered. The difference between curve a and b is that for curve b the additional heating by the nuclear energy is taken into account. Curve c was calculated, taking into acount in addition to the ohmic losses the nuclear energy deposited in the TF coil system see eq. (55)

With relation (53) the electric power is calculated for the refrigeration system necessary to cool down the TF system during two pulses to the inital temperature T_o. (The energy deposited in the TF magnet system as a function of T_o is given by Fig. 23.) The results are shown in Fig. 24. Curve a shows the electric power for the cooling system as a function of T_o for the TF system, where the cooling power P_c is calculated from curve a of Fig. 23 as $P_c(T_o) = E_{OH}(T_o)/3600$. Curve a in Fig. 23 shows the time-integrated (over the current cycle $0 < t < 20.5$) ohmic losses for the whole TF coil system for the case where the nuclear heating is not taken into account [$q_{n,\gamma} \equiv 0$ in eq. (3')] . Curve bof Fig. 24 shows the electric power calculated from the time-integrated ohmic losses (E_{OH} values of curve b of Fig. 23) for the whole TF coil system, but, unlike in curve a, with allowance for the influence of the nuclear heating. The increase results from the increased temperatures (see, for instance, Fig. 9), which produce higher $\rho_e(T)j^2$ values. Curve c of Fig. 24 was calculated from the E_{OH} values of curve b in Fig. 23 (including nuclear heating) and the nuclear energy deposited in the TF coil system. P_c for this case is given by

$$P_c(T_o) = [\, E_{OH}(T_o) + E_{n,\gamma} \,]/3600 \qquad (54)$$

with

$$E_{n,\gamma} = \int_{t_B} \int_V q_{n,\gamma} \cdot dt \cdot dV \qquad (55)$$

(t_B = burn time; V = volume of the TF system). The $E_{n,\gamma}$ value was found to be 216 MJ.

The curves of Fig. 24 have minima. These minima correspond to optimum temperatures T_o if the electric power for the cooling system is considered. The optimum initial temperature T_o is 44K for pulses without nuclear burning (curve a). If nuclear heating is included the optimum value for T_o is 70 K.

References

/1/ U. Broßmann, J.E. Gruber. W.D. Haubenberger, O. Jandl, M. Söll, B. Streibl: "Tape-wound Toroidal (TF) Magnet for ZEPHYR", Max-Planck-Institut für Plasmaphysik, Report IPP 1/176 (1979)

/2/ M. Söll: " Bending-Free Shapes for Toroidal Magnet System", Max-Planck-Institut für Plasmaphysik, Projekt Systemstudien, Interner Report No. 19

/3/ U. Broßmann, J.E. Gruber, W.D. Haubenberger, O. Jandl, F. Mast, M. Söll, B. Streibl: " Toroidal Field Magnet for ZEPHYR; Tape and Bitter Concepts Conductor and Insulation Materials", Internal ZEPHYR Report

/4/ A. Elsner: "Gedanken zur Kinetik und Thermodynamik der Verdampfung von LN2 bei der Abkühlung der ZEPHYR-Magneten", Max-Planck-Institut für Plasmaphysik, Report IPP 1/183 (1980)

/5/ H. Brockmann, H. Krause, U. Ohlig: "1D Radiation Analysis for the Fusion Ignition Experiment ZEPHYR", Max-Planck-Institut für Plasmaphysik, Report IPP 1/173 (1979).

/6/ H.S. Carslaw, J.C. Jaeger: "Conduction of Heat in Solids", Oxford University Press 1976

/7/ M.B. Kasen: "Mechanical and thermal properties of filamentary-reinford structural composites at cryogenic temperatures", Cryogenics (1975) 337

/8/ M. Söll, O. Jandl, M. Gorenflo: "Mechanical Stress Calculations for Toroidal Field Coils by the Finite Element Method", Max-Planck-Institut für Plasmaphysik, IPP 4/142 (1976)

/9/ H. Gorenflo, O. Jandl: "Calculation of the Nodal forces in the 20-node Isoparametric Three-Dimensional Solid Element by the SHAPE Computer Program", Max-Planck-Institut für Plasmaphysik, Report IPP 4/167 (1978)

/10/ H. Gorenflo, O. Jandl: "Mesh Generation for the 20-Node Isoparametric Solid Element by the Computer Program MESHGEN", Max-Planck-Institut für Plasmaphysik, Report IPP 4/148 (1977)

/11/ "Handbook on Materials for Superconducting Machinery", Metalls and Ceramics Information Center Battelle (1977)

/12/ BBC; private communication

Appendix I

Material data

The material data used for this study are shown in the following figures. Figure A1 shows the specific resistivity of copper with a residual resistivity ratio R = 100 and R = 30. The resistivity at point A (see Fig. 8 or 14) produced by the magneto-resistance ρ_{eB} is plotted in Fig. A1. It is obvious from Fig. A1 that for low temperatures T < 40 K the magneto-resistivity is the dominant part for high magnetic induction values (B > 10 T).

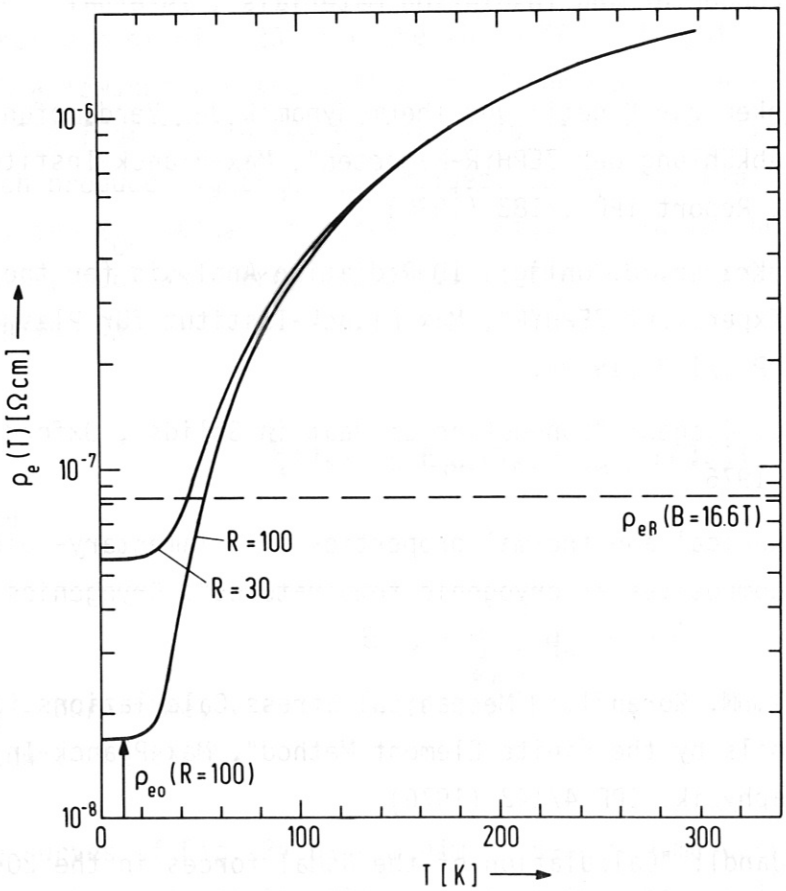

Fig. A1

Specific resistivity for copper with residual resistivity ratios R = 100 and 30

The specific heat functions per unit volume $\rho_m \cdot c(T)$ for copper and stainless steel S 310 are plotted in Fig. A3. They were produced from the specific heat data c per unit mass (J/kgK) /11/ and multiplied by $\rho_m = 8.9 \times 10^{-3}$ kg/cm^3 for copper and by 7.9×10^{-3} kg/cm^3 for stainless steel.

The temperature profiles in electrical insulation material (Sec. 2.2) were calculated by using the material data (Orlitherm) from Fig. A3 and A4.

The electrical insulation material Orlitherm was proposed by the firm of BBC/12/ in a study for the ZEPHYR toroidal magnet system.

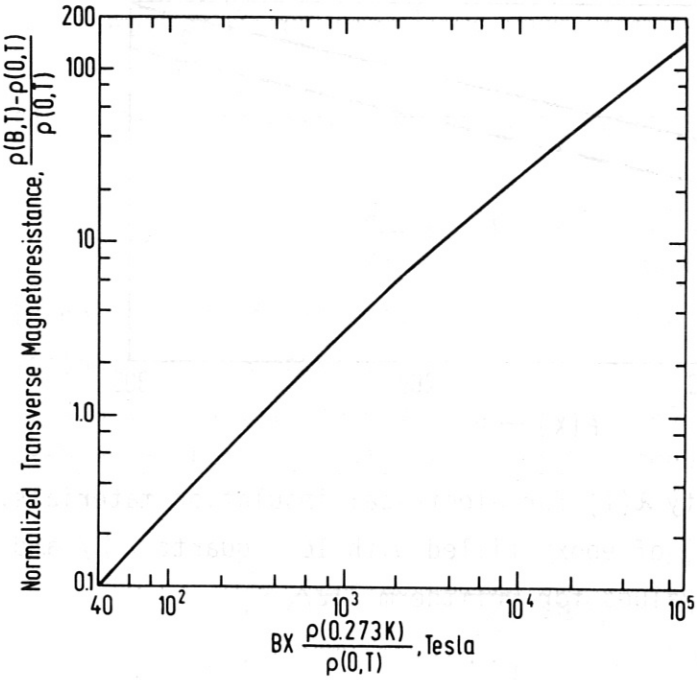

Fig. A2

Transverse (electrical) magneto-resistance of copper (reduced Kohler plot) /11/

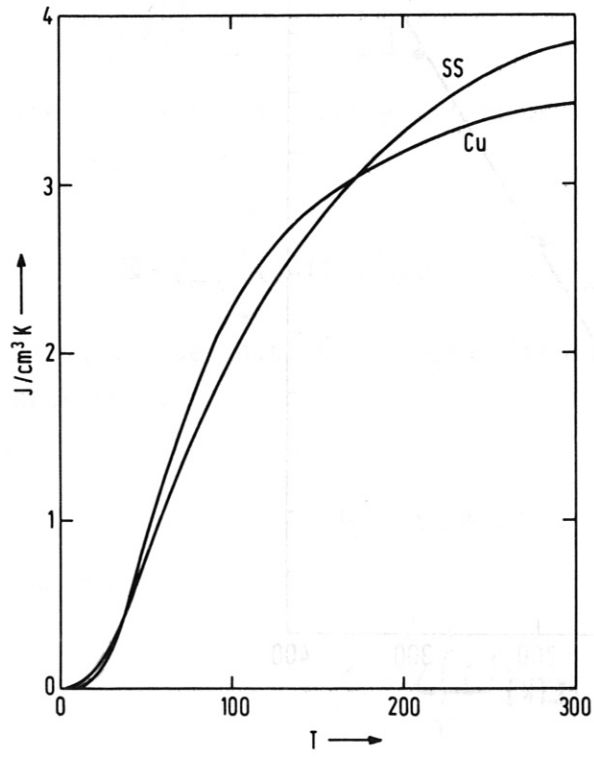

Fig. A3

Specific heat $\rho m \cdot c$ (T) for copper and stainless steel S 310 /11/

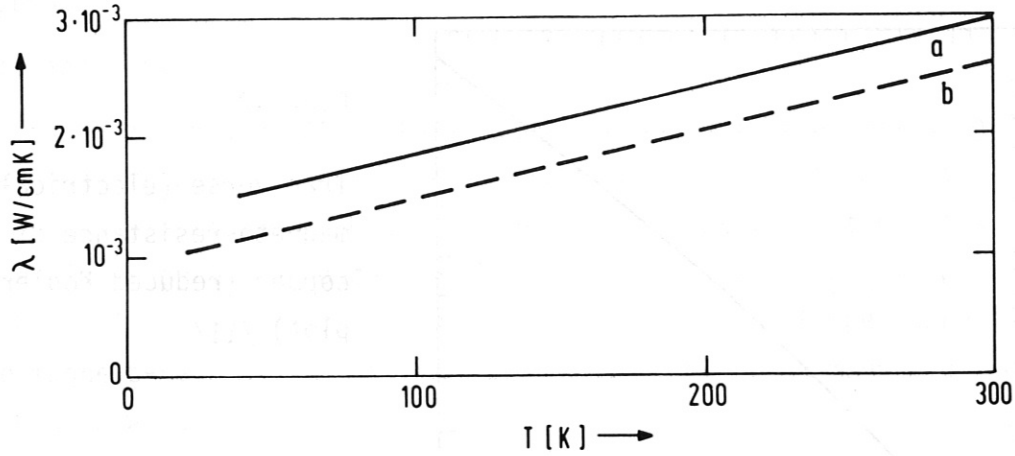

Fig. A4 Thermal conductivity $\lambda(T)$ for electrical insulation materials. Curve a shows λ (T) of epoxy filled with 16 % quartz / 7 / and curve b the λ (T) values for Orlitherm /12/

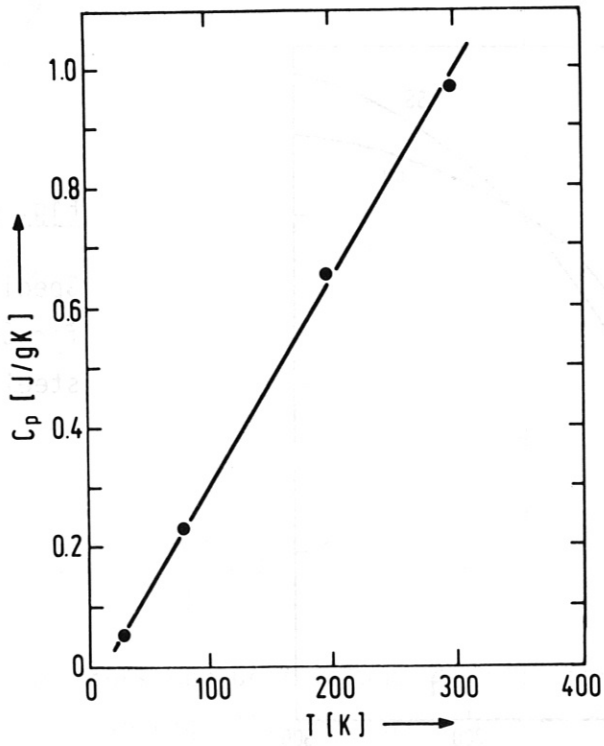

Fig. A5 Dependence of specific heat (values from BBC /11/ and the literature /7/)

Appendix II

"Heat equation" for a compound conductor

In adiabatic approximation the temperatures are calculated by

$$\frac{\partial T}{\partial t} = \frac{\rho_e}{\rho_m \cdot c} j^2 + \frac{q}{\rho_m \cdot c} \quad . \tag{A1}$$

In eq. (A1) it is assumed that the material heated by $\rho_e j^2$ and q is isotpoic and homogeneous.
We discuss in this appendix the changes which have to be carried out with respect to eq. (A1) if a compound conductor is used.

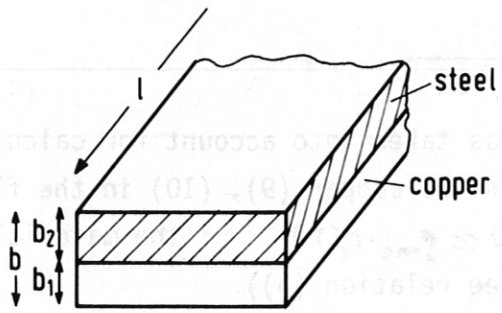

Fig. A6
Geometrical arrangement of a compound conductor consisting of copper and steel.

The heat absorbed by the conductor-assuming constant temperature in the conductor - is

$$Q = \rho_{mc} \int_{T_0}^{T} c_c(T') \cdot a \cdot b_1 \cdot l \cdot dT' + \rho_{ms} \int_{T_0}^{T} c_s(T') \cdot a \cdot b_2 \cdot l \cdot dT' \quad . \tag{A2}$$

Using the definition $\alpha = b_2/b_1$ (steel-copper ratio), b_1 and b_2 can be expressed by

$$b_1 = b/(1+\alpha) \; ; \quad b_2 = \alpha \cdot b/(1+\alpha) \quad , \tag{A3}$$

and Q by

$$Q = V \int_{T_0}^{T} \left[\frac{\rho_{mc} \cdot c_c}{(1+\alpha)} + \frac{\alpha \rho_{ms} c_s}{(1+\alpha)} \right] dT' \quad , \tag{A4}$$

where $V = a \cdot b \cdot l$.
The specific heat for the compound is found from A4 to be

$$\bar{c} = \rho_{mc} c_c/(1+\alpha) + \alpha \cdot \rho_{ms} \cdot c_s/(1+\alpha) \quad . \tag{A4}$$

The specific resistivity of the compound conductor is ($\rho_{es} \gg \rho_{ec}$)

$$\bar{\rho}_e = \rho_{ec}[1+\alpha] \quad . \tag{A5}$$

The term = $\rho_e j^2 / \rho_m C$ in eq. (A1) is changed for the compound conductor t_o

$$\frac{\rho_e j^2}{\rho_m \cdot c} = \frac{\rho_{ec}(1+\alpha)^2}{\rho_{mc} \cdot c_c + \alpha \rho_{ms} \cdot c_s} j^2 \quad , \tag{A6}$$

where j is the current density for the whole compound conductor with the cross-sectional area a·b.

To find an analytical approximation the "material function" $f = \rho_e / \rho_m \cdot c$ was calculated for $\alpha = 0$, $\alpha = 1$ and $\alpha = 2$ (see Fig. 3). The expression

$$f = \frac{\rho_{ec}}{\rho_{mc} \cdot c_c + \alpha \rho_{ms} c_s} \tag{A7}$$

was used. The coefficient ($1 + \alpha$) was taken into account for calculating the current density $j_o = j\ (1 + \alpha)$ in the copper (9), (10) in the flat-top phase. Figure A3 shows that $\rho_{mc} \cdot c_c(T) \approx \rho_{ms} \cdot c_s(T)$; the material function f hencecan be approximated by f_a (see relation (6)).

$$f_a \frac{\rho_{ec}}{\rho_{mc} \cdot c_c [1+\alpha]} \quad . \tag{A8}$$

Acknowledgement

The autor gratefully acknowledges the assistance of H. Gorenflo and D. Pohl who wrote and tested the TEVBA computer program.